Sensitivity of Block Copolymer Self-Assembly to the Modification of a Single Monomer

Sensitivity of Block Copolymer Self-Assembly to the Modification of a Single Monomer

By Desiree Rehel,

A Thesis Submitted to the School of Graduate Studies in the Partial Fulfillment of the Requirements for the Degree Master of Science

McMaster University

Master of Science (2024)

Hamilton, Ontario (Department of Physics and Astronomy)

TITLE: Sensitivity of Block Copolymer Self-Assembly to the Modification of a Single Monomer

AUTHOR: Desiree Rehel (McMaster University)

SUPERVISOR: Dr. An-Chang Shi

NUMBER OF PAGES: x, 85

Abstract

In this project, the sensitivity of the phase behaviour of AB diblock copolymers to the addition a single C-monomer is investigated using self-consistent mean-field theory. The reference diblock copolymers are composed of the minority A block with $N_{\mathrm{A}} = 12$ monomers and the majority B block with N_{B} monomers. The blocks are mutually repulsive and their interaction is characterised by χ_{ij} and acts over range σ_{ij}, where i and j represent the monomer species. When a C-monomer is added to the junction of the diblock copolymers, we observe a notable shift of the phase boundaries to the larger N_{B} and smaller χ_{AB}. The shift to larger N_{B} is due to an increased polymer stretching. When the C-monomers is nearly-neutral, the shift does not strongly depend on the interaction strength. Similarly, the shift is not visibly affected by changing σ_{AC} and σ_{BC}. However, when the the strength of the interaction is selective such that $\chi_{\mathrm{AC}} = \chi_{\mathrm{AB}} + \alpha$ and $\chi_{\mathrm{BC}} = \chi_{\mathrm{AB}} - \alpha$, the shift size decreases with increasing α. Conversely, when the selective C-monomer is added to the majority end, the phase boundaries are shifted to the smaller N_{B}, with the smallest α giving the largest shift. The shifts can be generically understood to be cause by the interplay between the changes in the interfacial tension and polymer stretching due to the C-monomer. These results demonstrate sensitivity of phase behaviour of AB diblock copolymers to the addition of a C-monomer and may provide a useful link between experiment and theory.

Acknowledgements

During my time at McMaster, I have been supported by many amazing people to whom I would like to express my sincere gratitude. First, I would like to thank my supervisor, Dr An-Chang Shi. You have been an amazing supervisor and I have learned so much from you. I really appreciate the time spent in conversation and your support throughout my degree. I would also like to thank the other members of our research group, Tom Lai, Jiayu Xie, Yu Li and Yang Yang, I have enjoyed working with all of you in various ways throughout my time at McMaster. I would especially like to thank Tom and Jiayu for the many conversations we had on many topics surrounding the research projects. Your time and effort is appreciated. I would like to thank Jiayu, for providing the base code that I modified for this project. I would also like to thank the members of my supervisory committee, Dr Paul Higgs and Dr Kari Dalnoki-Veress. I appreciate the time and feedback that you have given.

Further, I would like to thank my family for their support. You were always there, encouraging me and believing in me. I also want to thank the many friends outside of McMaster, including and especially, Jamie, Sneha, and Rachel. You all been such amazing friends and I appreciate your support.

Contents

List of Figures

List of Tables

Declaration of Contribution

I, Desiree Rehel, modified existing SCFT code that was provided by Dr. Jiayu Xie. I wrote relevant codes and scripts to submit jobs on the Digital Research alliance of Canada's computer clusters and to process the data. I also followed notes by Dr. Jiayu Xie and the PhD thesis of Dr. Chi To Lai in writing the theory chapter of the thesis. I wrote the entirety of the thesis, after which edits were made based on suggestions from Dr An-Chang Shi. Conclusions regarding the behaviour of the polymers were made through discussion with Dr. Shi.

Chapter 1

Introduction

1.1 What is Polymer

Polymers are long, flexible molecules composed of many covalently-bonded subunits, called monomers. It has been over 100 years since this understanding of polymers was first proposed by Staudinger in 1920 [1, 2]. In that 100 years, polymers, both synthetically produced and naturally occurring, have become an almost irreplaceable part of our everyday lives [1, 3, 4]. Naturally occurring polymers are present in and produced by living organisms, for example, the DNA and proteins found in living beings [5]. Moreover, both synthetically produced and naturally occurring polymers are used in many common objects such as plastics, rubbers, coatings, dental fillings, and more [1, 3, 4]. Combining these applications and natural occurrences of polymers, we find that polymers touch almost every aspect of our current way of life. [1, 3, 4]

Due to the ubiquity of polymers, it is expected that having a good understanding

of their properties and behaviour under a wide variety of conditions is desirable. One method to classify the widely-varying polymers is by their molecular properties. For example, a polymer may be classified by its chemical structure as either a homopolymer, composed of chemically identical monomers, or a heteropolymer, composed of least two chemically distinct types of monomers [2]. The arrangement of the distinct monomers in heteropolymers can vary from having large blocks of identical monomers connected, to arrangements of single monomer sequences [2]. Polymers containing two blocks of chemically distinct monomers are called diblock copolymers, while polymers containing three blocks are called triblock terpolymers, [2, 6]. Schematic illustrations of both homopolymers and select block copolymers are shown in Fig. 1.1.

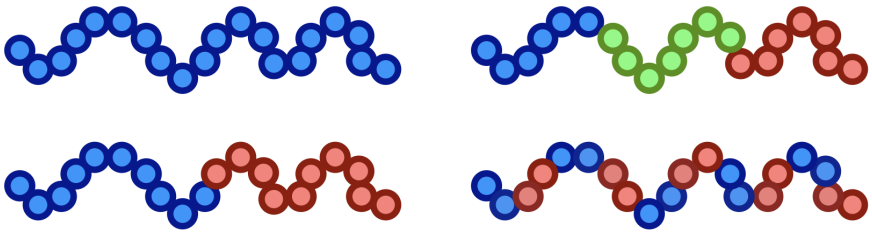

FIGURE 1.1: Schematic illustration of a homopolymer (top left) and several variations of heteropolymers.

Another characteristic of a polymer chain is its flexibility. One way in which the polymers flexibility is characterized is the Kuhn length, b, which is defined as the length over which the direction of the unit vectors tangent to the polymer become uncorrelated. A rigid polymer will have a large Kuhn length to total length ratio [7], and therefore, there is a high energetic cost to the chain bending along its contour.

This type of polymer will resemble a rod [7]. On the opposite end of the flexibility spectrum where the Kuhn length to total length ratio is small, there is very little energetic cost to the chain bending, and the polymer is considered fully-flexible [7]. This type of polymer will resemble a soft string. In between these two extremes where the polymer retains some resistance to bending but not so much so that it resembles a rod, the polymer is considered to be semi-flexible [7]. Illustrations of rigid, semi-flexible and fully flexible chains are shown in Fig. 1.2.

FIGURE 1.2: Illustration of polymer chains with varying degrees of flexibility.

A third defining feature of a polymer is its architecture. In Fig. 1.1, we only show linear polymers, or polymers whose monomers are all sequential from start to finish such that the polymer has two free ends. However, polymers may have a wide variety of architectures such as ring polymers, where the two ends of a linear polymer are covalently bonded together, star polymers, where three or more branches originate from a single point in the chain, and grafted polymers, where several branches are tethered to a linear backbone [2]. Some examples of different polymer architectures are displayed in Fig. 1.3.

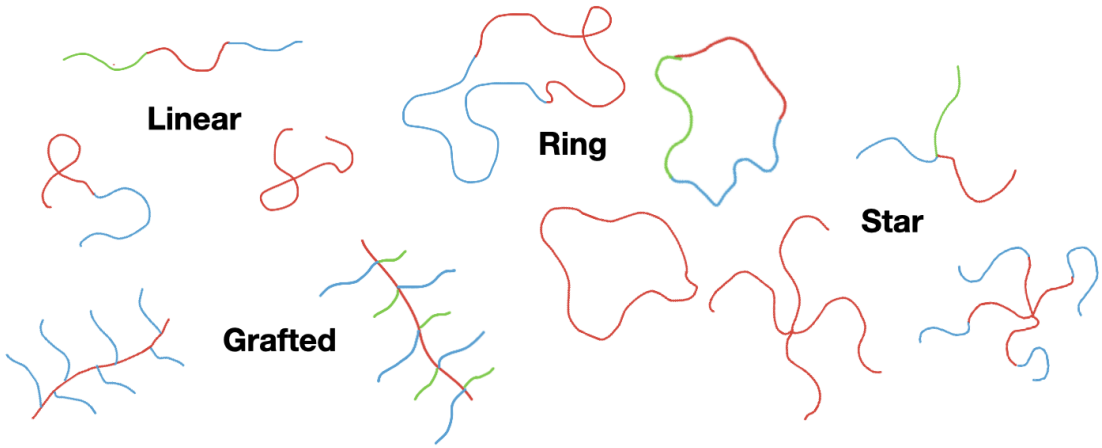

Figure 1.3: Schematic illustration of various polymer architectures for both homopolymers and heteropolymers

In this thesis, we are concerned with the behaviour of block copolymers. There are many ways to produce block copolymers [8–10]. The methods to obtain block copolymers typically fall into one of two categories [8, 10]: The first, known as controlled polymerization techniques, adds monomers in a sequential fashion to grow a chain. Some methods that fall under this category are atom transfer racial polymerization (ATRP) and radical addition-fragmentation chain transfer (RAFT) [10].

The second category that the production methods exploit reactions that bond the ends of two already-grown chains together [10]. One such highly efficient and important method in this category, albeit less versatile than some other methods, is the click method [9, 10]. In this method the end groups can either undergo a click reaction without modification or will be modified to be able to undergo the click reaction. This reaction bonds the blocks together and creates the diblock copolymer

[9]. One noteworthy consequence of this method is that there is small section of chain where the blocks join together that is distinct from both the A and B blocks.

1.2 Frustration and Self-Assembly of Block Copolymers

Now we turn our attention to the behaviour and characteristics of block copolymer melts, which is a fluid state where the monomer concentration is 100%. Due to the various, competing interactions in the system which cannot all be simultaneously be minimized, block copolymer melts are frustrated on several length scales [6]. On a molecular length scale, one force contributing to the frustration arises from the interactions between the monomers in the blocks. This interaction is characterised by the Flory-Huggins parameter, χ, defined as,

$$\chi = \frac{z}{2}\frac{2U_{\mathrm{AB}} - U_{\mathrm{AA}} - U_{\mathrm{BB}}}{kT}, \tag{1.1}$$

where U_{IJ} is the contact energy between monomers of type I and J [2], z is the number of nearest-neighbours, k is the Boltzmann constant and T is temperature. In many cases the chemically distinct blocks are mutually repulsive, resulting in a positive value of χ and the different blocks tending to separate. The second force contributing to the frustration on the molecular scale arises from the covalent bond that holds the distinct blocks together. This bond does not allow the polymer blocks to break apart and fully separate. Therefore, there is frustration in the system since the two energy

associated with these two forces cannot be simultaneously minimized [6].

In order to minimize the frustration on the molecular level, the polymers tend to segregate into structures known either as block copolymer assemblies or micelles, containing A-rich and B-rich regions [6, 11]. These micelles vary in shape from lamellae to cylinders to spheres depending on the characteristics of the block copolymers [6, 11, 12]. Some examples of what a micelle might look like are illustrated in Fig. 1.4.

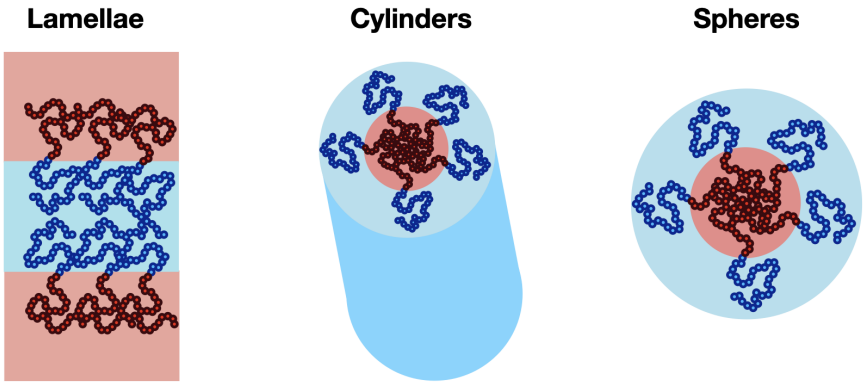

FIGURE 1.4: Illustration of some of the various possible micelle shapes.

Frustration present on larger length scales also partially determines the shape and packing of the micelles [6, 12]. Another contributing factor is that polymers behave as entropic springs, and therefore, there is a cost to chain stretching [6, 11, 12]. Finally, the interfacial energy, due to the polymer blocks being mutually repulsive, will also contribute to the frustration. [6, 11, 12]. These different and opposing interactions lead to frustrations in the system that must be balanced [6, 12].

By understanding the frustrations present, we can predict when different micelle shapes shown in Fig. 1.4 could be stabilized. First consider chains where one block is much shorter than the other. If these polymers were arranged with the blocks in a lamellar domain there would be a higher energetic cost for the longer block to stretch away from the interface [11]. Therefore, we expect interface to curve towards the shorter blocks [6, 11, 12] to relax the stretching of the longer block [11]. With a large length asymmetry between blocks, we expect spherical micelles to form [6, 11, 12]. Building on this, as the length of the blocks becomes more symmetric, the need for interfacial curvature lessens to allow the formation of cylinders and eventually, when the block are either symmetric or almost symmetric in length, lamellae. Overall, the predicted sequence with increasing the block-length asymmetry, is lamellar to cylinders to spheres [6, 11, 12]. It should be noted that micelles can also take other shapes, such as in bicontinuous structures which will be seen in later chapters [6, 11, 12].

There is another factor that contributes to the frustration at this length scale, the requirement of the monomers to completely fill space [6, 11, 12]. This along with the other factors, determine how the micelles are arranged with respect to each other. Of the micelles in Fig. 1.4, the only one that can fill space without deforming its shape is the lamellae micelle [6]. However, as mentioned above, there are situations where lamellae is not the ideal micelle shape to satisfy all other sources of frustration present in the system. In these situations, where we the cylindrical or spherical micelles are preferable, the micelles cannot pack in a way that fills space undeformed, as shown

in Fig. 1.5. Therefore, the micelle corona becomes distorted to that of the relevant Wigner-Sietz cell [6, 11] as illustrated in Fig. 1.5. Due to the cost of chain stretching, the distortion of the corona in turn distorts the shape of the core. This core distortion is less though and is determined by the rigidity of the blocks forming the corona [6, 11], as shown in Fig. 1.5. The deformed micelles can also vary in size and shape from other micelles in the same melt to allow optimum packing. Depending on the system parameters, these micelles can form various phases [6]. Some of the simpler examples being lamellar, hexagonally-packed cylinders, hexagonal close-packed spheres, and body centered cubic [6, 11].

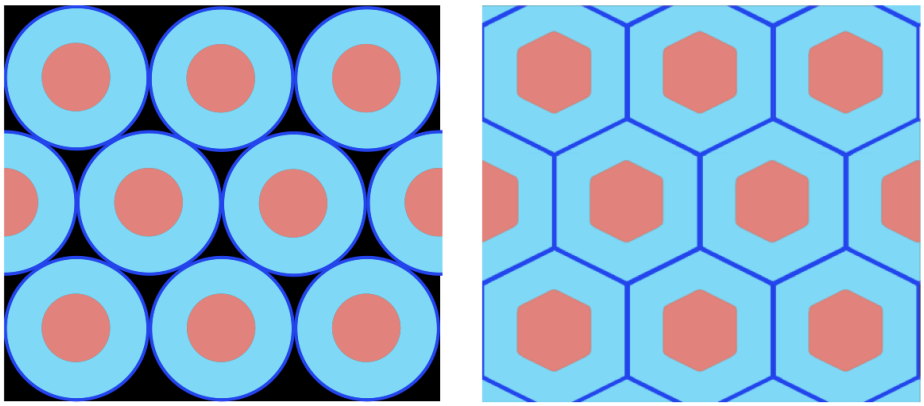

FIGURE 1.5: Illustration showing the distortion of cylindrical micelles in order to fill space when arranged in a hexagonal-closed-packed pattern. Left: undeformed cylinders unable to fill space. Right: cylindrical micelles deformed to fill space. Note: Cylinders are not drawn to scale.

Block copolymers and their self-assembly into complex structures have been studied, experimentally and theoretically, for many years with the first records dating back to the 1960s [10]. Since this time, the amount of interest, reflected in the number of

yearly papers mentioning diblock copolymers, has skyrocketed, from only a few in the 1960s to thousands in the 2010s [10].

One particular study in 1995 by Bates *et. al.* [13], examined the phase behaviour of polyisopropene-polystyrene diblock copolymers. While polyisopropene-polystyrene diblock copolymers had already been examined in other previous studies [14–18], most other studies had examined regions far from the the order-disorder transition (ODT) [13]. The ODT is where the stable phase of the melt transitions from one which exhibits microphase separation to one where the polymers are uniformly distributed and display no ordered structures (disordered). The phase diagram from this study is shown in Fig. 1.6 a) and contains 5 stable phases. Two of these phases are the double gyroid, or Ia$\bar{3}$d, phase that had recently been confirmed by Hadjuk *et al* in 1993 [17], and the ABC stacked hexagonally-perforated lamellar [13]. Another study by Winey *et al* in 1994 also predicted a similar phase diagram in the strong segregation limit and a similar location for the order-disorder transition. Backed by other recent research [13, 17, 19], Hadjuk *et. al.* also determined that another phase that had been reported, the ordered bicontinuous double diamond, was not a stable phase. They determined that previous studies reporting this phase to be stable likely confused it with the double gyroid phase due, in part, to the similarities between the two phases [13].

On the theoretical side, in 1994 Matsen and Schick [20] employed a spectral method of self-consistent field theory (SCFT) to theoretically study the phase behaviour of diblock copolymers whose A and B-block Kuhn length were identical [20–22]. The

resulting phase diagram is shown in Fig. 1.6 b). One difference between the studies is that in the theoretical study, the Kuhn lengths of the two block were equal, while in the experiment they were not. This conformational asymmetry between block plays an important role in the phase behaviour, and explains some of the discrepancies observed [23, 24]. One discrepancy seen is the presence of the PL phase in the experimental phase diagram, but not in the theoretical phase diagram. Later studies both experimentally [25] and theoretically [26] showed that the PL phase is a metastable transition state of AB diblock copolymer melts, not a thermodynamically stable phase [22]. Another discrepancy noted is that the ODT transitions in Fig. 1.6 a) are from various phases to disorder, while in 1.6 b)the are only from the cubic phases. This discrepancy can be explained by fluctuations that are not accounted for in SCFT [27]. Overall, the theoretical phase diagram agrees quite well with the experimental results in Fig. 1.6 a) from Ref [13].

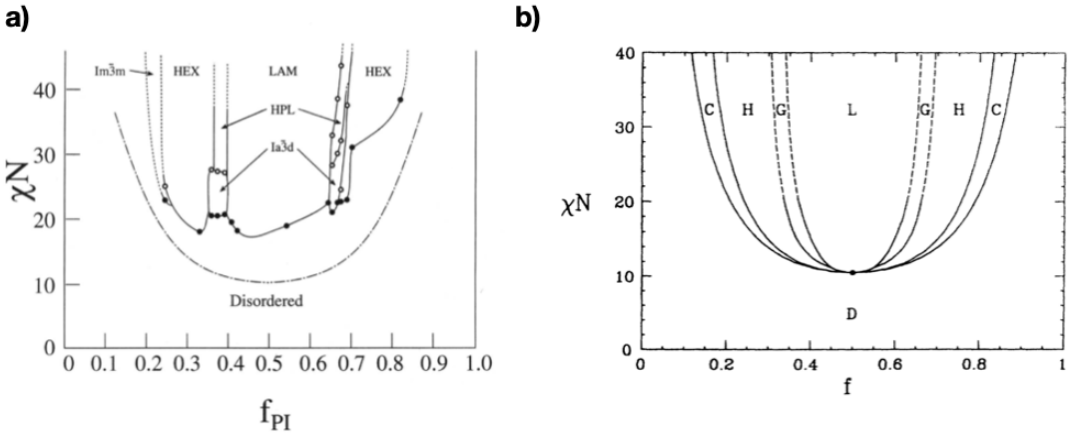

FIGURE 1.6: Phase diagrams of AB diblock copolymers. a) Experimentally obtained phase diagram of conformationally asymmetric PI-PS block copolymers from Ref. [13]. b) Theoretically obtained phase diagram of conformationally symmetric diblock copolymers from Ref. [21]. The phase labels are as follows: Lam=L=Lamellar, HEX=H=Hexagonally-packed cylinders, Ia3d=G=Double gyroid, D=Disordered, HPL=Hexagonally-perforated Lamellar, Im$\bar{3}$m=BCC, and C=cubic. Both of the diagrams are reproduced with permission from their publishers.

In the earlier studies, the spherical phases were found to be simple ones, such as BCC and HCP; however, there are other spherical phases that are more complex. One family of these complex spherical phases is the Frank-Kasper (FK) phases. These phases consist of micelles whose WS cells take the shape of 4 possible polyhedra with coordination numbers of 12, 14, 15, and 16 [28–30]. An illustration of these polyhedra are illustrated in Fig. 1.7, which is reproduced from Ref. [28]. When these polyhedra pack together they form tetrahedrally close packed phases and are called the Frank-Kasper phases [28–31].

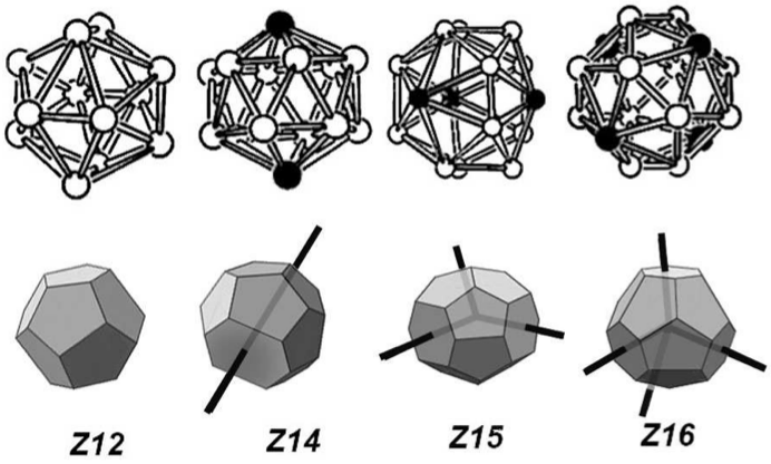

FIGURE 1.7: Illustration of the 4 Frank-Kasper polyhedra from Ref. [28]. Reproduced with permission from publisher

While the FK phases are commonly observed in metals, they have also been found in several soft matter systems [31]. In 2003, the FK A15 phase was found to be metastable in diblock copolymers and stable in branched copolymers [31, 32]. Later in 2010, Bates *et. al.*, found that the FK σ phase is stable in diblock copolymer melts [31, 33]. The two other FK phases found in copolymer systems are C14 and C15. Discovering FK phases in block copolymer systems is exciting because not only does it open new areas of potential research in what was thought to be a fairly well understood area, but it also provides a broad connection between the block copolymer systems and various other soft and hard matter systems that also for these phases [31]. These phases are equilibrium phases in some complex systems, such as in diblock copolymer blends, where polymers of different lengths are blended together, but not

in diblock copolymer melts where all of the constituent polymers have the same length [31]. Unit cells for these four FK phases, A15, σ, C14, and C15 are shown in Fig. 1.8.

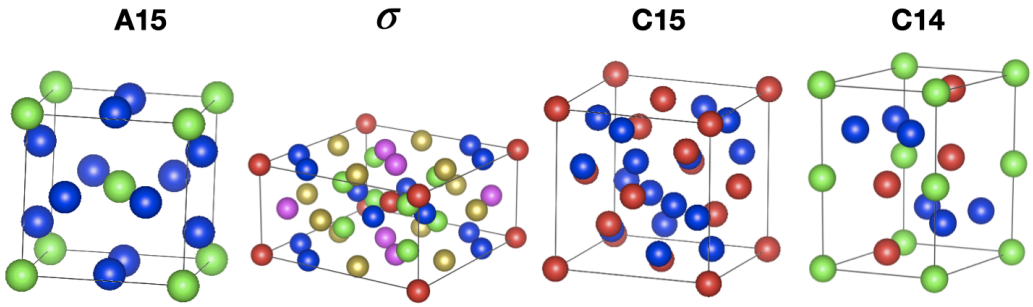

Figure 1.8: Unit cells of A15, σ, C15 and C14. The atoms, or micelles, colored according to their Wycoff numbers. Made with Vesta [34]

The phase behaviour of triblock copolymers is much more complex than that of diblock copolymers. The parameter space to be explored is much larger due to the extra parameters [6, 35, 36]. Due to this increase in complexity, there is currently no complete phase diagram for this type of melt [37]. In this discussion, we momentarily narrow focus, and examine the so-called nonfrustrated ABC systems. In these systems the order of monomer-monomer repulsion strengths is the same as the order of blocks along the contour of the chain, or $\chi_{AB}N \cong \chi_{BC}N < \chi_{AC}N$ for an ABC-type triblock terpolymer [6]. Therefore, the name nonfrustrated is because even though the previously-mentioned frustrations are clearly still present, the ordering of the repulsion strengths do not create any further frustration [6]. While there have been many studies on triblock terpolymers, one major contribution came from an

early experimental study by Bailey et al [38] on nonfrustrated diblock copolymers using Poly(isoprene-b-styrene-b-ethylene oxide). This study suggested the presence of a phase that became known as Fddd or O^{70} [35, 38–40]]. This was later confirmed experimentally by Epps *et. al.* in 2004 [40–42] and Tyler et al in 2005 using self-consistent field theory [39, 43]. This finding lead researchers to reexamine the phase diagram of simple diblock copolymer melts and find the Fddd phase to be stable in a narrow region of the diblock copolymer phase diagram [43].

A 2007 study by Tyler, Bates and Morse [35], continued examining the phase behaviour of nonfrustrated triblock copolymer melts using SCFT. This study produced complete phase diagrams for $\chi_{AB} = \chi_{BC} \ll \chi_{AC}$ for specific values of χ_{AB}, χ_{BC}, and χ_{AC} in the triangle of f_A, f_B, and f_C. One of resultant phase diagrams with $\chi_{AB}N = chi_{BC}N = 13$ and $\chi_{AC}N = 35$ is shown in Fig. 1.9. Looking along the edge in which the $f_B = 0$, and hence where the system is reduced a diblock copolymer melt, the progression of phases matches the progression found in Refs. [13] and [21], as expected. However, as the volume fraction of the C-block increases we see several new phases emerge, including the alternating gyroid (G^A) and the alternating diamond (D^A) phases. A later study by the same group [44], expanded this work to other values of $k = \chi_{AC}/\chi_{AB}$ to explore how the value of k affects the phase behaviour. They found, among other things, that for slightly asymmetric triblocks the Fddd remains stable [44].

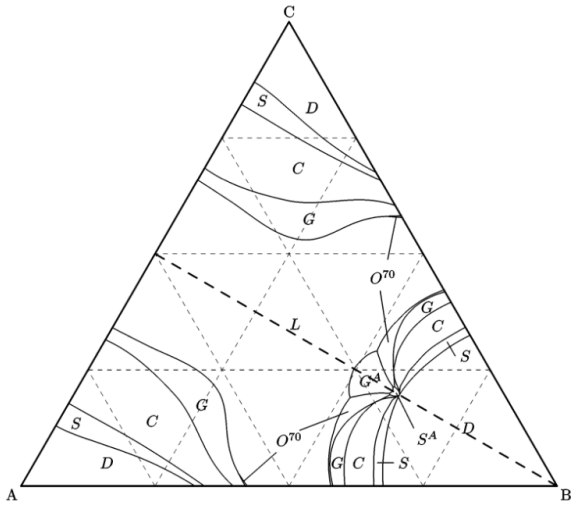

FIGURE 1.9: Phase diagram of a nonfrustrated triblock terpolymer melt for $\chi_{AB}N = chi_{BC}N = 13$ and $\chi_{AC}N = 35$ from Ref. [35]. Recreated with permission from publisher.

Now we briefly turn our attention to frustrated triblock copolymer systems where the order of the monomer-monomer repulsion do not align with the order of the blocks along the contour of the chain, $\chi_{AC} < \chi_{BC}$. In this type of melts, structures which place the B-monomers in smaller domains arranged around AC interfaces are preferred [6]. This arrangement leads to a larger number of structures available than what is seen in nonfrustrated systems [36]. One 2012 study by Liu. et al [37], examined the phase behaviour of frustrated ABC triblock copolymers melts using SCFT. In part of this study, they investigated the phase behaviour of a melt with parameters close to polystyrene-poly(ethylene-co-butylene)-poly(methyl methacrylate), otherwise known as PS-PEB-PMMMA. Several complex phases with two length scales were found, including lamellae in cylinders (LC) and perforated circular lamellar-on-cylinders (PC).

The phase diagram produced is shown in Fig. 1.10. Further, a theoretical study in 2012 by Li *et al* [45], found that helical superstructures emerge as the stable structure in some frustrated triblock terpolymer melts.

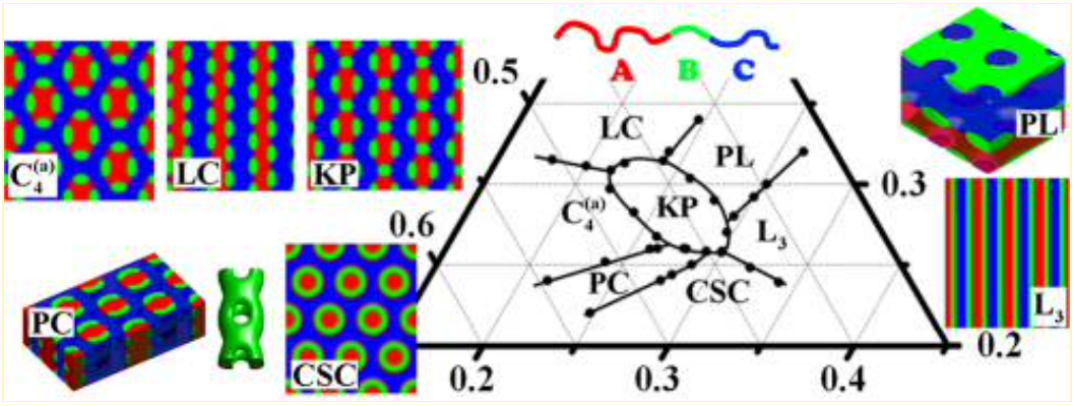

FIGURE 1.10: Frustrated triblock terpolymer partial phase diagram with parameters set to closely match those of PS-PEB-PMMMA, or with χ_{AB}N=40, χ_{BC}N=80, and χ_{AC}N=15 with ϵ_B=2.0 and ϵ_C=1.5. Recreated from [37] with permission from publisher.

Over the years there has been much progress in understanding the behaviour of block copolymers through many studies. Some have looked at developing methods, such as those described earlier, to synthesize block copolymers with various architectures [46–57]. Others have looked at the behaviour and structures these polymers form in various circumstances both experimentally and theoretically [12–19, 21, 23, 24, 26, 31–33, 35, 37, 44, 45, 58–66]. In a 2020 publication, the editors and advisory board of the journal, Macromolecular Chemistry and Physics, reflected on what the future of polymer science could look like[1]. Along with several other areas, the authors suggested sustainability as a possible major area of growth for polymers. One class

of polymer that fits the criteria of green polymers is sugar-based polymers [66], such as those examined in a recent study by Chen *et al* [66]. In this study, the authors examined the phase behaviour of sugar-based diblock copolymers that were fabricated by a click method. The observed order of phase transitions for the linear diblocks that were studied is Lamellar ->Hexagonally-Perforated Lamellar->Double Gyroid->Hexagonal Cylinders. Finding the Hexagonally-Perforated Lamellar phase to be thermodynamically stable is interesting as it is typically considered to be unstable in coil-coil diblock copolymer melts [22].

In many studies, the polymers examined are considered to be neat AB diblock or ABC triblock copolymers. This assumption overlooks the commonly-seen presence of different chemical structures at the junctions or at the ends of the polymers. In more recent years, this feature been investigated, not only to better understand its effects, but also as way of tuning the phase behaviour and morphology of the melts. A 2015 study by Hawker *et. al.* [67, 68], explored the effects of introducing an ionic junction in diblock copolymers and found the ODT temperature significantly affected by the junction. Another study in 2017 [69] examined the effects of introducing hydrogen bonding to the junction of PS-b-PMMA diblock copolymers. They found that the interfacial width and line roughness were both decreased by the introduction of the introduction of hydrogen bonding [68, 69]. Further studies such as Refs. [70, 71] have also studied the effects of changing the junctions, finding that the phase behaviour, ODT temperature and domain spacing of the resultant phases can all be notably effected.

Further, single C-monomers can also be found or placed at the ends of the block copolymers. There are several studies that clearly demonstrate the versatility of using this strategy to tune their phase behaviour [68, 72]. There have been several experimental studies exploring this effect, such as a 2013 study by Park *et. al.* [72, 73] which clearly demonstrated that the phase behaviour of diblock copolymers can be tuned by modifying the end groups of PS-b-PEO diblock copolymers with either SO_3H or SO_3Li. They found that the modification leads to an increase in block segregation and allows the formation of the double gyroid phase, where the melt would otherwise be disordered [68, 72, 73]. Similarly a 2017 [74] study noted that desirable cocontiuous phase could be formed by modifying the end-groups using click reactions [68, 72, 74]. More recently a study [72, 75] examined the effects of adding diphosponic end groups to PS-b-PEO block copolymers using either ether or amine linkers. By using the amine linker, the researchers stabilized the Fddd and Ia$\bar{3}d$ phases, and by using the ether linker, the double-plumbers nightmare were stabilized [72, 75].

1.3 Thesis Motivation

Due to the prevalence of polymers in our everyday world, understanding the behaviours of diblock copolymers is relevant to many areas. Recently, exploring the effects of adding one C-type monomer to either the ends or the junctions of block copolymers has become an area of interest since the C-monomers are often present as a result of the experimental methods used to synthesize the polymer and could

provide an efficient way to tune and modify the resultant phase behaviour [68]. While there has been several experimental studies on these types of systems, many theoretical studies overlook the possibility of the junctions or polymer ends being different. Therefore, in this thesis, we fill this gap and further our understanding of the effects of adding a single C-monomer by examining the sensitivity of the phase behaviour of AB diblock copolymers to the addition of a C-type monomer either to one of the ends of the polymer or to the junction using SCFT.

1.4 Notation

In this thesis, we examine the phase behaviour of AB diblock copolymer that have a C-monomer added to either the junction of the polymer or to one of the ends. In order to avoid long descriptions, we will use the following notation:

- A will always refer to the minority block.
- B will always refer to the majority block.
- The single C-monomer will be denoted with a lowercase c to indicate that it is only a single monomer.
- The position of the blocks and C-monomer will be indicated by the ordering of the name.

For example, a A-c-B block copolymer is an AB diblock copolymer with a C-monomer added to the junction. Note, we have also added in dashes for neatness.

1.5 Organization of the Thesis

The rest of the thesis is organized as follows: Chapter two gives an overview of the methods and relevant theoretical background. Chapter 3 presents the main results for A-c-B type polymers. Chapter 4 presents the main results for A-B-c type polymers. Finally Chapter 5 brings everything together to discuss the main conclusions and possible future work.

Chapter 2

Theory

2.1 Polymer models

Over the years, several polymer models have emerged with various levels of detail. In many cases the chemical structure of the polymers in question are known, and thus one could, in principle, account for them in the model. However, adding such details to the polymer model comes at a significant computational cost. Therefore, many models are coarse-grained, meaning many of the chemical details are ignored, only retaining the main overall features describing the polymers. Some of these models describe the polymers in a discrete manner, where all of the monomer positions are specified [76]. These types of models can incorporate various interactions between beads [76]. Two examples of such models would be the discrete Gaussian chain model and the freely-jointed chain (FJC). The main difference between these models is the nature of the bonded interaction between the monomers. In the Gaussian chain model,

the monomers are connected by Gaussian springs, while in the FJC model the beads are connected by freely-rotating, rigid rods [76]. Both of these models are illustrated in Fig. 2.1.

Other polymer models fall into the continuous class of models. Here the polymer is described by some continuous path $\vec{R}(s)$, where s the position along the contour of the chain. One common and useful model in this class is the continuous Gaussian chain model. In this model the polymer is modelled as linearly elastic when stretched, and fully flexible [76]. Another, continuous model, the wormlike chain, describes the polymer as a semi-flexible, continuous path that cannot be stretched [76]. An illustration of these models is shown in Fig. 2.1.

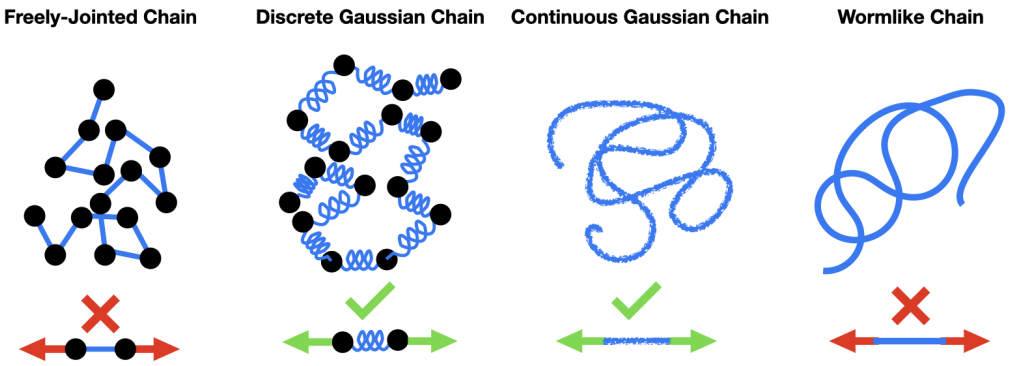

FIGURE 2.1: Labelled illustrations of different polymer models. Below each model the illustration illustrates if the polymer can be stretched on short length scales.

Applying the FJC model to diblock or triblock copolymers is straightforward. Now, instead of having just a single bond length, we will have a bond length for each of the

blocks and another bond length for the bond between the blocks. We can also vary the interactions between the different types of bead pairs, and potentially three different monomer volumes. An illustration of diblock and triblock copolymers modelled as FJCs is shown in Fig. 2.2

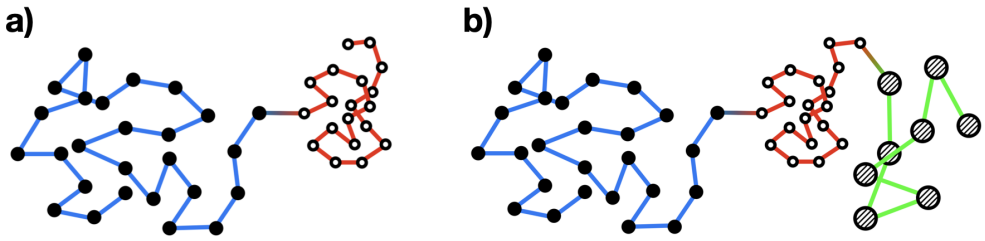

FIGURE 2.2: Illustration of the freely-jointed chain model of a) diblock copolymers and b) a triblock terpolymer

The downfall to using coarse-grained models is that there is some inherently information lost about any behaviour of the polymers that come from to their specific chemical structure. Typically though, this is valid since we are generally interested in the global behaviours that are insensitive to the molecular details. In this thesis, we employ the freely-jointed chain model with N_i monomers joined by bonds of length b_i, where the subscript i indicates the monomer or bond type. We choose the bond length of the C-monomers, and the bonds between any two types of monomers was taken to be equal to b_{A} and the bond length between two B monomers was taken to be $0.5b_{\mathrm{A}}$. Further, we have chosen the same volumes for the all monomer types.

2.2 Triblock terpolymers in a melt

The polymers considered in this thesis are a limiting case of triblock copolymers, where one block has only one C-type segment. Therefore, in this section we derive the self-consistent mean-field equations for ABC triblock terpolymer melts, which can then be directly applied to this project. When examining the statistical properties of any system, one very useful quantity is the partition function of the system [77], defined as,

$$Z = \mathrm{Tr}(\mathrm{e}^{-\beta H(\vec{p},\vec{r})}) \tag{2.1}$$

where $\beta = k_{\mathrm{B}}T$, H is the Hamiltonian of the system, $\vec{r}$ and $\vec{p}$ are the relevant position and momenta coordinates, and the trace is over the energy eigenstates of the Hamiltonian. Extending this to a freely jointed chain with N particles and therefore $N-1$ bonds, we obtain [76–78],

$$Z_0 = \int d\vec{r}^{N} \exp(-\beta H(\vec{r}^{N})) \tag{2.2}$$

where the integral is over all possible particle positions and H is the Hamiltonian of the polymer with the configuration given by the N position vectors of the particles.

In order to derive the SCFT equations, we first need to specify the partition function of a the triblock copolymers melt. First, we define our Hamiltonian, which will

contain 2 parts: the part dues to the bond interactions, and the part due to the non-bonded interactions. We first consider the bond component. In the FJC model, each type of bond can only have one length, b, therefore, the bond-length distribution is a delta function [78],

$$\mathcal{P}(\vec{R}) = \frac{1}{4\pi b^2}\delta(\vec{R} - b) = \exp(-\beta H_{\text{bond},1}(\vec{R})),$$

where $H_{\text{bond},1}$ is the Hamiltonian associated with the bond energy attributed to a single bond. Rearranging, we obtain,

$$H_{\text{bond},1} = -kT \ln\left(\frac{1}{4\pi b^2}\delta(\vec{R} - b)\right).$$

The extension to a melt with n polymers with N bonds yields [78]

$$H_{\text{bond}} = -kT \sum_{j=1}^{n}\left(\sum_{i=1}^{N} \ln\left(\frac{1}{4\pi b_i^2}\delta(\vec{R}_{j,i} - b_i)\right)\right), \tag{2.3}$$

where $\vec{R}_j^i = \vec{r}_j{}^i - \vec{r}_j{}^{i-1}$ is the vector pointing from the ith monomer to the $i-1$th monomer in the jth chain and b_i is the relevant bond length between the $i-1$th and the ith monomers and may change along the chain.

To consider the non-bonded component, we first define the density operators for each of the monomer types [78],

$$\hat{\phi}_{\text{A}}(\vec{r}) = \sum_{j=1}^{n}\sum_{i=1}^{N_{\text{A}}} \delta(\vec{r} - \vec{r}_{j,i}), \tag{2.4}$$

$$\hat{\phi}_{\mathrm{B}}(\vec{r}) = \sum_{j=1}^{n} \sum_{i=N_{\mathrm{A}}+1}^{N_{\mathrm{B}}} \delta(\vec{r} - \vec{r}_{j,i}), \tag{2.5}$$

$$\hat{\phi}_{\mathrm{C}}(\vec{r}) = \sum_{j=1}^{n} \sum_{i=N_{\mathrm{B}}+1}^{N_{\mathrm{C}}} \delta(\vec{r} - \vec{r}_{j,i}). \tag{2.6}$$

It is of note that the above expressions have been simplified by employing the assumption that v_{A}, v_{B}, and v_{C} are all 1.

The non-bonded interactions between monomers of type α and β are then given by the Flory-Huggins interaction [78],

$$kT\chi_{\alpha,\beta} \int u_{\alpha\beta}(|\vec{r} - \vec{r}'|)\hat{\phi}_{\alpha}(\vec{r})\hat{\phi}_{\beta}(\vec{r}')d\vec{r}d\vec{r}', \tag{2.7}$$

where α and β can be A, B, or C but $\alpha \neq \beta$, and $u_{\alpha\beta}(|\vec{r} - \vec{r}'|)$ is typically given by [78],

$$u_{\alpha\beta}(R) = \left(\frac{3}{2\pi\sigma_{\alpha\beta}^2}\right)^{3/2} \exp\left(-\frac{3R^2}{2\sigma_{\alpha\beta}^2}\right) \tag{2.8}$$

with $R = |\vec{r} - \vec{r}'|$. Therefore, we find the non-bonded component of the Hamiltonian to be,

$$\begin{aligned} H_{\mathrm{nb}} =& kT\chi_{\mathrm{AB}} \int u_{\mathrm{AB}}(|\vec{r} - \vec{r}'|)\hat{\phi}_{\mathrm{A}}(\vec{r})\hat{\phi}_{\mathrm{B}}(\vec{r}')d\vec{r}d\vec{r}' \\ &+ kT\chi_{\mathrm{AC}} \int u_{\mathrm{AC}}(|\vec{r} - \vec{r}'|)\hat{\phi}_{\mathrm{A}}(\vec{r})\hat{\phi}_{\mathrm{C}}(\vec{r}')d\vec{r}d\vec{r}' \\ &+ kT\chi_{\mathrm{BC}} \int u_{\mathrm{BC}}(|\vec{r} - \vec{r}'|)\hat{\phi}_{\mathrm{B}}(\vec{r})\hat{\phi}_{\mathrm{C}}(\vec{r}')d\vec{r}d\vec{r}' \end{aligned} \tag{2.9}$$

and the complete Hamiltonian, excluding the irrelevant kinetic energy component [77], becomes,

$$\begin{aligned} H =& - kT \sum_{j=1}^{n} \sum_{i=0}^{N} \ln \left(\frac{1}{4\pi b_i^2} \delta(\vec{R_{j,i}} - b) \right) \\ &+ kT\chi_{\mathrm{AB}} \int u_{\mathrm{AB}}(|\vec{r} - \vec{r}'|) \hat{\phi}_{\mathrm{A}}(\vec{r}) \hat{\phi}_{\mathrm{B}}(\vec{r}') d\vec{r} d\vec{r}' \\ &+ kT\chi_{\mathrm{AC}} \int u_{\mathrm{AC}}(|\vec{r} - \vec{r}'|) \hat{\phi}_{\mathrm{A}}(\vec{r}) \hat{\phi}_{\mathrm{C}}(\vec{r}') d\vec{r} d\vec{r}' \\ &+ kT\chi_{\mathrm{BC}} \int u_{\mathrm{BC}}(|\vec{r} - \vec{r}'|) \hat{\phi}_{\mathrm{B}}(\vec{r}) \hat{\phi}_{\mathrm{C}}(\vec{r}') d\vec{r} d\vec{r}' \end{aligned} \tag{2.10}$$

From this, the configurational partition function of an n chain melt in the canonical ensemble is [78],

$$\begin{aligned} Z =& \frac{1}{n!} \prod_{j=1}^{n} \int d\vec{r}_j^N \exp \Bigg\{ -\beta H_{\mathrm{bond}} \\ &- \chi_{\mathrm{AB}} \int u_{\mathrm{AB}}(|\vec{r} - \vec{r}'|) \hat{\phi}_{\mathrm{A}}(\vec{r}) \hat{\phi}_{\mathrm{B}}(\vec{r}') d\vec{r} d\vec{r}' \\ &- \chi_{\mathrm{AC}} \int u_{\mathrm{AC}}(|\vec{r} - \vec{r}'|) \hat{\phi}_{\mathrm{A}}(\vec{r}) \hat{\phi}_{\mathrm{C}}(\vec{r}') d\vec{r} d\vec{r}' \\ &- \chi_{\mathrm{BC}} \int u_{\mathrm{BC}}(|\vec{r} - \vec{r}'|) \hat{\phi}_{\mathrm{B}}(\vec{r}) \hat{\phi}_{\mathrm{C}}(\vec{r}') d\vec{r} d\vec{r}' \Bigg\}, \end{aligned} \tag{2.11}$$

where, for simplicity we have used H_{bond} in place of Eq. 2.3.

Now our goal is to change it the form of the partition function from one where we integrate over positions to one where we integrate over fields so that the SCFT approximation can be applied. The first step is apply the identity [76, 78],

$$1 = \int \mathcal{D}\phi_\alpha(\vec{r}) \delta[\phi_\alpha(\vec{r}) - \hat{\phi}_\alpha(\vec{r}], \tag{2.12}$$

to Eq. 2.11 for each of the three types of monomers:

$$
\begin{aligned}
Z = \frac{1}{n!}\prod_{j=1}^{n}\int d\vec{r}_j^{N}\int \mathcal{D}\phi_A(\vec{r})\int \mathcal{D}\phi_B(\vec{r})\int \mathcal{D}\phi_C(\vec{r})\\
\delta[\phi_A(\vec{r})-\hat{\phi}_A(\vec{r})]\delta[\phi_B(\vec{r})-\hat{\phi}_B(\vec{r})]\delta[\phi_C(\vec{r})-\hat{\phi}_C(\vec{r})]\\
\exp\Bigg\{-\beta H_{\text{bond}}-\chi_{\text{AB}}\int u(|\vec{r}-\vec{r}'|)\hat{\phi}_{\text{A}}(\vec{r})\hat{\phi}_{\text{B}}(\vec{r}')d\vec{r}d\vec{r}'\\
-\chi_{\text{AC}}\int u(|\vec{r}-\vec{r}'|)\hat{\phi}_{\text{A}}(\vec{r})\hat{\phi}_{\text{C}}(\vec{r}')d\vec{r}d\vec{r}'-\chi_{\text{BC}}\int u(|\vec{r}-\vec{r}'|)\hat{\phi}_{\text{B}}(\vec{r})\hat{\phi}_{\text{C}}(\vec{r}')d\vec{r}d\vec{r}'\Bigg\}.
\end{aligned}
$$

Now we take advantage of the delta functional identity [76, 78],

$$
\delta[\phi_\alpha(\vec{r})-\hat{\phi}_\alpha(\vec{r})]=\int \mathcal{D}\omega_\alpha \exp\left(\iota\int d\vec{r}\omega_\alpha[\phi_\alpha(\vec{r})-\hat{\phi}_\alpha(\vec{r})]\right) \tag{2.13}
$$

to obtain,

$$
\begin{aligned}
Z = \frac{1}{n!}\prod_{j=1}^{n}\int d\vec{r}_j^{N}\int \mathcal{D}\phi_A(\vec{r})\int \mathcal{D}\phi_B(\vec{r})\int \mathcal{D}\phi_C(\vec{r})\int \mathcal{D}\omega_A\int \mathcal{D}\omega_B\int \mathcal{D}\omega_C\\
\exp\left(\iota\int d\vec{r}\omega_A[\phi_\alpha(\vec{r})-\hat{\phi}_A(\vec{r})]\right)\exp\left(\iota\int d\vec{r}\omega_B[\phi_\alpha(\vec{r})-\hat{\phi}_B(\vec{r})]\right)\\
\exp\left(\iota\int d\vec{r}\omega_C[\phi_\alpha(\vec{r})-\hat{\phi}_C(\vec{r})]\right)\exp\Bigg\{-\beta H_{\text{bond}}\\
-\chi_{\text{AB}}\int u(|\vec{r}-\vec{r}'|)\hat{\phi}_{\text{A}}(\vec{r})\hat{\phi}_{\text{B}}(\vec{r}')d\vec{r}d\vec{r}'-\chi_{\text{AC}}\int u(|\vec{r}-\vec{r}'|)\hat{\phi}_{\text{A}}(\vec{r})\hat{\phi}_{\text{C}}(\vec{r}')d\vec{r}d\vec{r}'\\
-\chi_{\text{BC}}\int u(|\vec{r}-\vec{r}'|)\hat{\phi}_{\text{B}}(\vec{r})\hat{\phi}_{\text{C}}(\vec{r}')d\vec{r}d\vec{r}'\Bigg\},
\end{aligned}
$$

where ω_α is the real conjugate field to ϕ_α and is interpreted as the chemical potential field. Now, using the definition of the density operator and absorbing the ι into the

conjugate fields we obtain,

$$
\begin{aligned}
Z = \frac{1}{n!} \int \mathcal{D}\phi_A(\vec{r}) \int \mathcal{D}\phi_B(\vec{r}) \int \mathcal{D}\phi_C(\vec{r}) \int \mathcal{D}\omega_A \int \mathcal{D}\omega_B \int \mathcal{D}\omega_C \\
\exp\Bigg\{ \int d\vec{r} \phi_{\mathrm{A}}(\vec{r})\omega_{\mathrm{A}}(\vec{r}) + \int d\vec{r} \phi_{\mathrm{B}}(\vec{r})\omega_{\mathrm{B}}(\vec{r}) + \int d\vec{r} \phi_{\mathrm{C}}(\vec{r})\omega_{\mathrm{C}}(\vec{r}) \\
- \chi_{\mathrm{AB}} \int u(|\vec{r}-\vec{r}'|)\hat{\phi}_{\mathrm{A}}(\vec{r})\hat{\phi}_{\mathrm{B}}(\vec{r}')d\vec{r}d\vec{r}' - \chi_{\mathrm{AC}} \int u(|\vec{r}-\vec{r}'|)\hat{\phi}_{\mathrm{A}}(\vec{r})\hat{\phi}_{\mathrm{C}}(\vec{r}')d\vec{r}d\vec{r}' \\
- \chi_{\mathrm{BC}} \int u(|\vec{r}-\vec{r}'|)\hat{\phi}_{\mathrm{B}}(\vec{r})\hat{\phi}_{\mathrm{C}}(\vec{r}')d\vec{r}d\vec{r}' \Bigg\} \\
\prod_{j=1}^{n} \int d\vec{r}_j^N \exp\Bigg\{ -\beta H_{\mathrm{bond}} - \sum_{i=1}^{N_{\mathrm{A}}} \omega_{\mathrm{A}}(\vec{r}_{j,i}) - \sum_{i=N_{\mathrm{A}+1}}^{N_B} \omega_{\mathrm{B}}(\vec{r}_{j,i}) - \sum_{i=N_{\mathrm{B}+1}}^{N_C} \omega_{\mathrm{C}}(\vec{r}_{j,i}) \Bigg\}.
\end{aligned}
\tag{2.14}
$$

Defining the normalized single chain partition function, [76, 78]

$$
Q = \frac{Z_1[\omega_{\mathrm{A}}, \omega_{\mathrm{B}}, \omega_{\mathrm{C}}]}{Z_1[0,0,0]}, \tag{2.15}
$$

with $Z_1[\omega_{\mathrm{A}}, \omega_{\mathrm{B}}, \omega_{\mathrm{C}}]$ as the partition function of a single chain in the fields ω_{A}, ω_{B} and ω_{C},

$$
Q \times Z_1[0,0,0] = \int d\vec{r}_j^N \exp\Bigg\{ -\beta H_{\mathrm{bond}} - \sum_{i=1}^{N_{\mathrm{A}}} \omega_{\mathrm{A}}(\vec{r}_{j,i}) - \sum_{i=N_{\mathrm{A}+1}}^{N_B} \omega_{\mathrm{B}}(\vec{r}_{j,i}) - \sum_{i=N_{\mathrm{B}+1}}^{N_C} \omega_{\mathrm{C}}(\vec{r}_{j,i}) \Bigg\}. \tag{2.16}
$$

But $Z_1[0,0,0]$, is a constant and therefore will not actually need to be calculated, and therefore, we exclude it. Finally, adding in $\eta(\vec{r})$ as a Lagrange multiplier to enforce

incompressibility, we obtain,

$$
\begin{aligned}
Z = \frac{1}{n!}\int \mathcal{D}\phi_A(\vec{r})\int \mathcal{D}\phi_B(\vec{r})\int \mathcal{D}\phi_C(\vec{r})\int \mathcal{D}\omega_A\int \mathcal{D}\omega_B\int \mathcal{D}\omega_C \\
Q^n \exp\Bigg\{\int d\vec{r}\phi_{\mathrm{A}}(\vec{r})\omega_{\mathrm{A}}(\vec{r}) + \int d\vec{r}\phi_{\mathrm{B}}(\vec{r})\omega_{\mathrm{B}}(\vec{r}) + \int d\vec{r}\phi_{\mathrm{C}}(\vec{r})\omega_{\mathrm{C}}(\vec{r}) \\
- \chi_{\mathrm{AB}}\int u(|\vec{r}-\vec{r}'|)\hat{\phi}_{\mathrm{A}}(\vec{r})\hat{\phi}_{\mathrm{B}}(\vec{r}')d\vec{r}d\vec{r}' - \chi_{\mathrm{AC}}\int u(|\vec{r}-\vec{r}'|)\hat{\phi}_{\mathrm{A}}(\vec{r})\hat{\phi}_{\mathrm{C}}(\vec{r}')d\vec{r}d\vec{r}' \\
- \chi_{\mathrm{BC}}\int u(|\vec{r}-\vec{r}'|)\hat{\phi}_{\mathrm{B}}(\vec{r})\hat{\phi}_{\mathrm{C}}(\vec{r}')d\vec{r}d\vec{r}' - \int d\vec{r}\eta(\vec{r})(1-\phi_{\mathrm{B}}(\vec{r})-\phi_{\mathrm{A}}(\vec{r})-\phi_{\mathrm{C}}(\vec{r}))\Bigg\}
\end{aligned}
\tag{2.17}
$$

.

Now by applying Sterlings approximation, $n! = (n/e)^n$, $n = V/N$, where V is the total volume of the system, and employing the definition of the Helmholtz free energy, we can define the free energy functional per chain [78],

$$
\begin{aligned}
\frac{F}{nkT} = \ln Q - \ln(\frac{e}{n}) - \frac{1}{V}\Bigg\{\int d\vec{r}N\phi_{\mathrm{A}}(\vec{r})\omega_{\mathrm{A}}(\vec{r}) + \int d\vec{r}N\phi_{\mathrm{B}}(\vec{r})\omega_{\mathrm{B}}(\vec{r}) \\
+ \int d\vec{r}N\phi_{\mathrm{C}}(\vec{r})\omega_{\mathrm{C}}(\vec{r}) - \chi_{\mathrm{AB}}N\int u(|\vec{r}-\vec{r}'|)\hat{\phi}_{\mathrm{A}}(\vec{r})\hat{\phi}_{\mathrm{B}}(\vec{r}')d\vec{r}d\vec{r}' \\
- \chi_{\mathrm{AC}}N\int u(|\vec{r}-\vec{r}'|)\hat{\phi}_{\mathrm{A}}(\vec{r})\hat{\phi}_{\mathrm{C}}(\vec{r}')d\vec{r}d\vec{r}' - \chi_{\mathrm{BC}}N\int u(|\vec{r}-\vec{r}'|)\hat{\phi}_{\mathrm{B}}(\vec{r})\hat{\phi}_{\mathrm{C}}(\vec{r}')d\vec{r}d\vec{r}' \\
- \int d\vec{r}\eta(\vec{r})(1-\phi_{\mathrm{B}}(\vec{r})-\phi_{\mathrm{A}}(\vec{r})-\phi_{\mathrm{C}}(\vec{r}))\Bigg\},
\end{aligned}
\tag{2.18}
$$

where we have absorbed N into the definition of $\eta(\vec{r})$.

Now, we note that there is a more convenient and intuitive way to express Q. To see this, start with Eq. (2.15) [78],

$$\begin{aligned} Q &= \frac{\int d\vec{r}^N \prod_{i=1}^{N-1} \exp\Big\{-\beta H_{\text{bond},1}(\vec{R}_i)\Big\} \prod_{i=1}^{N} \exp\Big\{-\omega(\vec{r}_i)\Big\}}{V\Big(\int d\vec{r}^N \exp\Big\{-\beta H_{\text{bond},1}(\vec{R})\Big\}\Big)^{N-1}} \\ &= \frac{1}{V}\int d\vec{r}^N \prod_{i=1}^{N-1} \frac{\exp\Big\{-\beta H_{\text{bond},1}(\vec{R}_i)\Big\}}{V\int d\vec{r}^N \exp\Big\{-\beta H_{\text{bond},1}(\vec{R})\Big\}} \prod_{i=1}^{N} \exp\Big\{-\omega(\vec{r}_i)\Big\} \\ &= \frac{1}{V}\int d\vec{r}^N e^{-\omega(\vec{r}_N)} g(\vec{r}_N - \vec{r}_{N-1}) e^{-\omega(\vec{r}_{N-1})} g(\vec{r}_{N-1} - \vec{r}_{N-2}) e^{-\omega(\vec{r}_{N-2})} g(\vec{r}_{N-2} - \vec{r}_{N-3}) \\ &...e^{-\omega(\vec{r}_3)} g(\vec{r}_3 - \vec{r}_2) e^{-\omega(\vec{r}_2)} g(\vec{r}_2 - \vec{r}_1) e^{-\omega(\vec{r}_1))}, \end{aligned} \tag{2.19}$$

where $g(\vec{r}_{i+1} - \vec{r}_i)$ is the normalized bond transition probability [78],

$$g(\vec{r}_{i+1} - \vec{r}_i) = \frac{\delta(\vec{r}_{i+1} - \vec{r}_i - b)}{4\pi b^2}, \tag{2.20}$$

with Fourier transform,

$$g(k) = \frac{\sin(kb)}{kb}. \tag{2.21}$$

Therefore, defining the forward integrated chain propagator with [76, 78],

$$q(\vec{r}_1, 1) = e^{-\omega(\vec{r}_1)}, \tag{2.22}$$

and

$$q(\vec{r}_{i+1}, i+1) = e^{-\omega(\vec{r}_{i+1})} \int d\vec{r}_i g(\vec{r}_{i+1} - \vec{r}_i) q(\vec{r}_i, i), \tag{2.23}$$

we obtain [78],

$$Q = \frac{1}{V} \int d\vec{r}_N q(\vec{r}_N, N). \tag{2.24}$$

Similarly, we define the backwards integrated what propagator [78],

$$q^\dagger(\vec{r}_N, N) = e^{-\omega(\vec{r}_N)}, \tag{2.25}$$

and

$$q^\dagger(\vec{r}_{i-1}, i-1) = e^{-\omega(\vec{r}_{i-1})} \int d\vec{r}_i g(\vec{r}_i - \vec{r}_{i-1}) q(\vec{r}_i, i), \tag{2.26}$$

we obtain [78],

$$Q = \frac{1}{V} \int d\vec{r}_N q^\dagger(\vec{r}_N, N). \tag{2.27}$$

2.3 Self-consistent field theory

If the expressions of the partition function could be evaluated exactly, we would be done; however, that is not the case [76]. Therefore, in order to obtain solutions, we assume the functional integrals are mainly governed by a single set of chemical potential fields; [11, 76]; this assumption is the mean-field approximation. The mean-field approximation leads to a set of self-consistent equations that need to be solved. Solutions of the the mean-field equations can be approximately obtained analytically in a few cases such as in the strong segregation regime [6, 11, 22, 76, 79], by using

theories such as those developed by Semenov[22, 79, 80], and in the weak segregation regime using theories such as the random phase approximation developed by Leibler [11, 22, 76, 79, 81]. To solve for the free energy in general, numerical methods have been developed and used widely including the work reported in this thesis. In this method, we numerically solve the self-consistent field equations to obtain the set of fields that minimize the free energy functional with respect to the monomer density fields, auxiliary fields, and Lagrange multipliers [11, 76, 78].

Taking the functional derivative with respect to ϕ_{A}, ϕ_{B}, and ϕ_{C} and setting those to zero in order to minimize the free energy yields,

$$\frac{\delta f}{\delta \phi_{\mathrm{A}}(\vec{r})} = -\frac{1}{V}(N\omega_{\mathrm{A}} - \chi_{\mathrm{AB}}N\int u(|\vec{r}-\vec{r'}|)\phi_{\mathrm{B}}d\vec{r'} - \chi_{\mathrm{AC}}N\int u(|\vec{r}-\vec{r'}|)\phi_{\mathrm{C}}d\vec{r'} + \eta(\vec{r})) = 0,$$

$$\frac{\delta f}{\delta \phi_{\mathrm{B}}(\vec{r})} = -\frac{1}{V}(N\omega_{\mathrm{B}} - \chi_{\mathrm{AB}}N\int u(|\vec{r}-\vec{r'}|)\phi_{\mathrm{A}}d\vec{r'} - \chi_{\mathrm{BC}}N\int u(|\vec{r}-\vec{r'}|)\phi_{\mathrm{C}}d\vec{r'} + \eta(\vec{r})) = 0,$$

and

$$\frac{\delta f}{\delta \phi_{\mathrm{C}}(\vec{r})} = -\frac{1}{V}(N\omega_{\mathrm{C}} - \chi_{\mathrm{BC}}N\int u(|\vec{r}-\vec{r'}|)\phi_{\mathrm{B}}d\vec{r'} - \chi_{\mathrm{AC}}N\int u(|\vec{r}-\vec{r'}|)\phi_{\mathrm{A}}d\vec{r'} - \eta(\vec{r})) = 0.$$

with $f = F/nkT$. Leading to,

$$N\omega_{\mathrm{A}} = \chi_{\mathrm{AB}}N\int u(|\vec{r}-\vec{r'}|)\phi_{\mathrm{B}}(\vec{r'})d\vec{r'} + \chi_{\mathrm{AC}}N\int u(|\vec{r}-\vec{r'}|)\phi_{\mathrm{C}}(\vec{r'})d\vec{r'} + \eta(\vec{r}) \quad (2.28)$$

$$N\omega_{\mathrm{B}} = \chi_{\mathrm{AB}}N\int u(|\vec{r}-\vec{r'}|)\phi_{\mathrm{A}}(\vec{r'})d\vec{r'} + \chi_{\mathrm{BC}}N\int u(|\vec{r}-\vec{r'}|)\phi_{\mathrm{C}}(\vec{r'})d\vec{r'} + \eta(\vec{r}) \quad (2.29)$$

$$N\omega_{\rm C} = \chi_{\rm BC} N \int u(|\vec{r}-\vec{r'}|)\phi_{\rm B}(\vec{r'})d\vec{r'} + \chi_{\rm AC} N \int u(|\vec{r}-\vec{r'}|)\phi_{\rm C}(\vec{r'})d\vec{r'} + \eta(\vec{r}) \tag{2.30}$$

The derivative with respect to $\eta(\vec{r})$ simply yields,

$$1 = \phi_{\rm A}(\vec{r}) + \phi_{\rm B}(\vec{r}) + \phi_{\rm C}(\vec{r}). \tag{2.31}$$

Finally, the derivative with respect to auxiliary fields yeild,

$$\frac{\delta f}{\delta \omega_{\rm A}(\vec{r})} = -\frac{\delta \ln Q}{\delta \omega_{\rm A}(\vec{r})} - \frac{N}{V}\phi_{\rm A} = 0,$$

$$\frac{\delta f}{\delta \omega_{\rm B}(\vec{r})} = -\frac{\delta \ln Q}{\delta \omega_{\rm B}(\vec{r})} - \frac{N}{V}\phi_{\rm B} = 0,$$

$$\frac{\delta f}{\delta \omega_{\rm B}(\vec{r})} = -\frac{\delta \ln Q}{\delta \omega_{\rm B}(\vec{r})} - \frac{N}{V}\phi_{\rm B} = 0.$$

To complete the above expression, we still need $\frac{\delta \ln Q}{\delta \omega_{\rm B}(\vec{r})}$. This is easy to obtain from Eqs. 2.23, 2.24, 2.26, and 2.27 as,

$$\frac{\delta \ln Q}{\delta \omega_{\rm B}(\vec{r})} = -\frac{e^{\omega_{\rm A}(\vec{r})}}{V} \sum_{i=1}^{N_{\rm A}} q(r_i, i) q^{\dagger}(r_i, i), \tag{2.32}$$

thus yielding,

$$\phi_{\rm A} = \frac{e^{\omega_{\rm A}(\vec{r})}}{QN} \sum_{i=1}^{N_{\rm A}} q(r_i, i) q^{\dagger}(r_i, i), \tag{2.33}$$

$$\phi_{\rm B} = \frac{e^{\omega_{\rm B}(\vec{r})}}{QN} \sum_{i=N_{\rm A}+1}^{N_{\rm B}} q(r_i, i) q^{\dagger}(r_i, i), \tag{2.34}$$

$$\phi_{\rm C} = \frac{e^{\omega_{\rm C}(\vec{r})}}{QN} \sum_{i=N_{\rm B}+1}^{N_{\rm C}} q(r_i, i) q^{\dagger}(r_i, i). \tag{2.35}$$

All together, we obtain the self-consistent field equations:

$$\begin{aligned}
1 &= \phi_{\mathrm{A}} + \phi_{\mathrm{B}} + \phi_{\mathrm{C}} \\
N\omega_{\mathrm{A}} &= \chi_{\mathrm{AB}} N \int u(|\vec{r} - \vec{r}'|)\phi_{\mathrm{B}} d\vec{r'} + \chi_{\mathrm{AC}} N \int u(|\vec{r} - \vec{r}'|)\phi_{\mathrm{C}} d\vec{r'} + \eta(\vec{r}) \\
N\omega_{\mathrm{B}} &= \chi_{\mathrm{AB}} N \int u(|\vec{r} - \vec{r}'|)\phi_{\mathrm{A}} d\vec{r'} + \chi_{\mathrm{BC}} N \int u(|\vec{r} - \vec{r}'|)\phi_{\mathrm{C}} d\vec{r'} + \eta(\vec{r}) \\
N\omega_{\mathrm{C}} &= \chi_{\mathrm{BC}} N \int u(|\vec{r} - \vec{r}'|)\phi_{\mathrm{B}} d\vec{r'} + \chi_{\mathrm{AC}} N \int u(|\vec{r} - \vec{r}'|)\phi_{\mathrm{C}} d\vec{r'} + \eta(\vec{r}) \\
\phi_{\mathrm{A}} &= \frac{e^{\omega_{\mathrm{A}}(\vec{r})}}{QN} \sum_{i=1}^{N_{\mathrm{A}}} q(r_i, i) q^{\dagger}(r_i, i) \\
\phi_{\mathrm{B}} &= \frac{e^{\omega_{\mathrm{B}}(\vec{r})}}{QN} \sum_{i=N_{\mathrm{A}}+1}^{N_{\mathrm{B}}} q(r_i, i) q^{\dagger}(r_i, i) \\
\phi_{\mathrm{C}} &= \frac{e^{\omega_{\mathrm{C}}(\vec{r})}}{QN} \sum_{i=N_{\mathrm{B}}+1}^{N_{\mathrm{C}}} q(r_i, i) q^{\dagger}(r_i, i)
\end{aligned} \tag{2.36}$$

Additionally, in the calculations we perform, we allow the box parameters, θ_{box}, to be vary, therefore, we will also need to minimize the stress of the system, which is defined as,

$$\begin{aligned}
\frac{\delta f}{\delta \theta_{\mathrm{box}}} = \sum_h \sum_k \sum_l \Bigg\{ & \chi_{\mathrm{AB}} \frac{du_{\mathrm{AB}}(\vec{G}_{hkl})}{dk^2} \frac{dk^2}{d\theta_{\mathrm{box}}} \hat{\phi}_{\mathrm{A}}(\vec{G}_{hkl}) \hat{\phi}_{\mathrm{B}}(\vec{G}_{hkl}) \\
& + \chi_{\mathrm{AC}} \frac{du_{\mathrm{AC}}(\vec{G}_{hkl})}{dk^2} \frac{dk^2}{d\theta_{\mathrm{box}}} \hat{\phi}_{\mathrm{A}}(\vec{G}_{hkl}) \hat{\phi}_{\mathrm{C}}(\vec{G}_{hkl}) \\
& + \chi_{\mathrm{BC}} \frac{du_{\mathrm{BC}}(\vec{G}_{hkl})}{dk^2} \frac{dk^2}{d\theta_{\mathrm{box}}} \hat{\phi}_{\mathrm{B}}(\vec{G}_{hkl}) \hat{\phi}_{\mathrm{C}}(\vec{G}_{hkl}) \\
& + \frac{dg(\vec{G}_{hkl})}{dk^2} \frac{dk^2}{d\theta_{\mathrm{box}}} \sum_{i=1}^{N-1} \hat{q}(\vec{G}_{hkl}, i) \hat{q}^{\dagger}(\vec{G}_{hkl}, i+1) \Bigg\}
\end{aligned} \tag{2.37}$$

where $\hat{q}$ is Fourier transform of q and G_{hkl} is a the reciprocal lattice vector defined by h, k, and l.

2.4 Numerical procedure

Now that we have the theoretical background and necessary equations, we will briefly outline the numerical procedure, called pseudo-spectral SCFT, and steps used in implementation.

1. Initialise the monomer density fields and box dimensions to be approximately that of the desired phase. In this project, we examined 13 phases, however, sometimes a few of the phases would not converge for a given set of parameters. The candidate phases examined are shown below. It should be noted however that not all phases were run for each point. Generally, all of the phases were run for the lowest value of $\chi_A B$ and the highest value of $\chi_A B$ and then at least 2 other values on the phase diagram. All other values, only had the phases that showed up in those 4 other values run.

2. Initialise the chemical potential fields from $\phi_{\mathrm{A}}(\vec{r})$, $\phi_{\mathrm{B}}(\vec{r})$, and $\phi_{\mathrm{C}}(\vec{r})$ using,

$$\omega_{\mathrm{A}}(\vec{r}) = \chi_{\mathrm{AB}}\phi_{\mathrm{B}}(\vec{r}) + \chi_{\mathrm{AC}}\phi_{\mathrm{C}}(\vec{r})$$
$$\omega_{\mathrm{B}}(\vec{r}) = \chi_{\mathrm{AB}}\phi_{\mathrm{A}}(\vec{r}) + \chi_{\mathrm{BC}}\phi_{\mathrm{C}}(\vec{r})$$
$$\omega_{\mathrm{C}}(\vec{r}) = \chi_{\mathrm{BC}}\phi_{\mathrm{B}}(\vec{r}) + \chi_{\mathrm{AB}}\phi_{\mathrm{A}}(\vec{r}).$$

It is to be stressed that the above equations are only used for computational convenience in the first step, as they only give an approximation to the fields and are not an accurate relation between the chemical potential fields and the monomer density profiles.

3. Using the current chemical potential fields and monomer density profiles, obtain the forward- and backward-integrated propagators, $q(\vec{r},i)$ and $q^{\dagger}(\vec{r},i)$, given by Eqs. 2.23 and 2.26. Once $q(\vec{r},i)$ and $q^{\dagger}(\vec{r},i)$ are obtained, use a Fourier transform to obtain $q(\vec{k},i)$ and $q^{\dagger}(\vec{k},i)$.

4. Using Eqs. 2.33, 2.34, and 2.35, calculate $\phi_{\mathrm{A}}(\vec{r})$, $\phi_{\mathrm{B}}(\vec{r})$, and $\phi_{\mathrm{C}}(\vec{r})$.

5. Obtain the Fourier transforms, $\phi_{\mathrm{A}}(\vec{k})$, $\phi_{\mathrm{B}}(\vec{k})$, $\phi_{\mathrm{C}}(\vec{k})$, $\omega_{\mathrm{A}}(\vec{k})$, $\omega_{\mathrm{B}}(\vec{k})$, and $\omega_{\mathrm{C}}(\vec{k})$.

6. Now we need to compute $\eta(\vec{r})$. By rearranging Eqs. 2.28, 2.29, 2.30, we obtain

$$\eta(\vec{r}) = \frac{1}{3}\Big(N\omega_{\mathrm{A}}(\vec{r}) + N\omega_{\mathrm{B}}(\vec{r}) + N\omega_{\mathrm{C}}(\vec{r}) + \chi_{\mathrm{AB}}\int u_{\mathrm{AB}}(|\vec{R}-\vec{r}'|)(1-\phi_{\mathrm{C}}(\vec{r}')) + \chi_{\mathrm{AC}}\int u_{\mathrm{AC}}(|\vec{R}-\vec{r}'|)(1-\phi_{\mathrm{B}})(\vec{r}') + \chi_{\mathrm{BC}}\int u_{\mathrm{AC}}(|\vec{R}-\vec{r}'|)(1-\phi_{\mathrm{A}}(\vec{r}'))\Big).$$

Now, take the Fourier transform and add in $\lambda(1-\phi_{\rm A}(\vec{k})-\phi_{\rm B}(\vec{k})-\phi_{\rm C}(\vec{k}))$ to encourage faster convergence, with λ is a numerical value:

$$\begin{aligned}\eta(\vec{k}) = \frac{1}{3}\Big(&N\omega_{\rm A}(\vec{k}) + N\omega_{\rm B}(\vec{k}) + N\omega_{\rm C}(\vec{k}) + N\chi_{\rm AB}\int u_{\rm AB}(k)(\delta(\vec{k})-\phi_{\rm C}(\vec{k})) \\ &+ N\chi_{\rm AC}\int u_{\rm AC}(k)(\delta(\vec{k})-\phi_{\rm B})(\vec{k}') + N\chi_{\rm BC}\int u_{\rm AC}(k)(\delta(\vec{k})-\phi_{\rm A}(\vec{k}))\Big) \\ &+ \lambda(1-\phi_{\rm A}(\vec{k})-\phi_{\rm B}(\vec{k})-\phi_{\rm C}(\vec{k}))\end{aligned} \tag{2.38}$$

Use this equation now to evaluate $\eta(\vec{k})$

7. Evaluate the new chemical potential fields using

$$N\omega_{\rm A}^{out}(\vec{k}) = \chi_{\rm AB}Nu_{\rm AB}(\vec{k})\phi_{\rm B}(\vec{k}) + \chi_{\rm AC}Nu_{\rm AC}(\vec{k})\phi_{\rm C}(\vec{k}) + \eta(\vec{k}) \tag{2.39}$$

$$N\omega_{\rm B}^{out}(\vec{k}) = \chi_{\rm AB}Nu_{\rm AB}(\vec{k})\phi_{\rm A}(\vec{k}) + \chi_{\rm BC}Nu_{\rm BC}(\vec{k})\phi_{\rm C}(\vec{k}) + \eta(\vec{k}) \tag{2.40}$$

$$N\omega_{\rm C}^{out}(\vec{k}) = \chi_{\rm AC}Nu_{\rm AC}(\vec{k})\phi_{\rm A}(\vec{k}) + \chi_{\rm BC}Nu_{\rm BC}(\vec{k})\phi_{\rm B}(\vec{k}) + \eta(\vec{k}), \tag{2.41}$$

and using a backward Fourier transform to calculate $\omega_{\rm A}^{out}(\vec{r})$, $\omega_{\rm B}^{out}(\vec{r})$, and $\omega_{\rm C}^{out}(\vec{r})$.

8. Find the residuals for the chemical potential fields, defined by,

$$\begin{aligned}d\omega_{\rm A}(\vec{r}) &= \omega_{\rm A}^{out}(\vec{r}) - \omega_{\rm A}(\vec{r}) \\ d\omega_{\rm B}(\vec{r}) &= \omega_{\rm B}^{out}(\vec{r}) - \omega_{\rm B}(\vec{r}) \\ d\omega_{\rm C}(\vec{r}) &= \omega_{\rm C}^{out}(\vec{r}) - \omega_{\rm C}(\vec{r})\end{aligned} \tag{2.42}$$

and for the lattice parameters, defined by,

$$d\theta_{\text{box}} = -\frac{df}{d\theta_{\text{box}}}\Delta\theta_{\text{box}}, \tag{2.43}$$

where $\Delta\theta_{\text{box}}$ is chosen to have some numerical value.

9. Update the chemical potential fields and the lattice parameters using either simple mixing for the first 5000 steps or Anderson afterward, as described in appendix A.

10. Calculate the free energy

$$\begin{aligned} F = &-\ln Q - N\sum_{\vec{k}}(\omega_{\text{A}}(\vec{k})\phi_{\text{A}}(\vec{k}) + \omega_{\text{B}}(\vec{k})\phi_{\text{B}}(\vec{k}) + \omega_{\text{C}}(\vec{k})\phi_{\text{C}}(\vec{k}) \\ &- \chi_{\text{AB}}u_{\text{AB}}(\vec{k})\phi_{\text{A}}(\vec{k})\phi_{\text{B}}(\vec{k}) - \chi_{\text{AC}}u_{\text{AC}}(\vec{k})\phi_{\text{A}}(\vec{k})\phi_{\text{C}}(\vec{k}) - \\ &\chi_{\text{BC}}u_{\text{BC}}(\vec{k})\phi_{\text{B}}(\vec{k})\phi_{\text{C}}(\vec{k})) \end{aligned} \tag{2.44}$$

and the error

$$Err = \left(\frac{\sum_{\vec{r}}(d\omega_{\text{A}}^2 + d\omega_{\text{B}}^2 + d\omega_{\text{C}}^2)}{\sum_{\vec{r}}(\omega_{\text{A}}^2 + \omega_{\text{B}}^2 + \omega_{\text{C}}^2)}\right) \tag{2.45}$$

11. If the criteria of Eq. 2.46 is not satisfied, go back to step 3 using the chemical potential fields and monomer density profiles from step 9 as inputs. Repeat this process until the desired accuracy is obtained.

$$
\begin{aligned}
&Max[|1-\phi_{\mathrm{A}}(\vec{r})-\phi_{\mathrm{B}}(\vec{r}]-\phi_{\mathrm{C}}(\vec{r}))\leq 10^{-7}\\
&Err\leq 10^{-5}\\
&\Delta F\leq 10^{-8}\\
&dL_{\mathrm{x,box}}\leq 10^{-5}\\
&dL_{\mathrm{y,box}}\leq 10^{-5}\\
&dL_{\mathrm{z,box}}\leq 10^{-5}
\end{aligned}
\tag{2.46}
$$

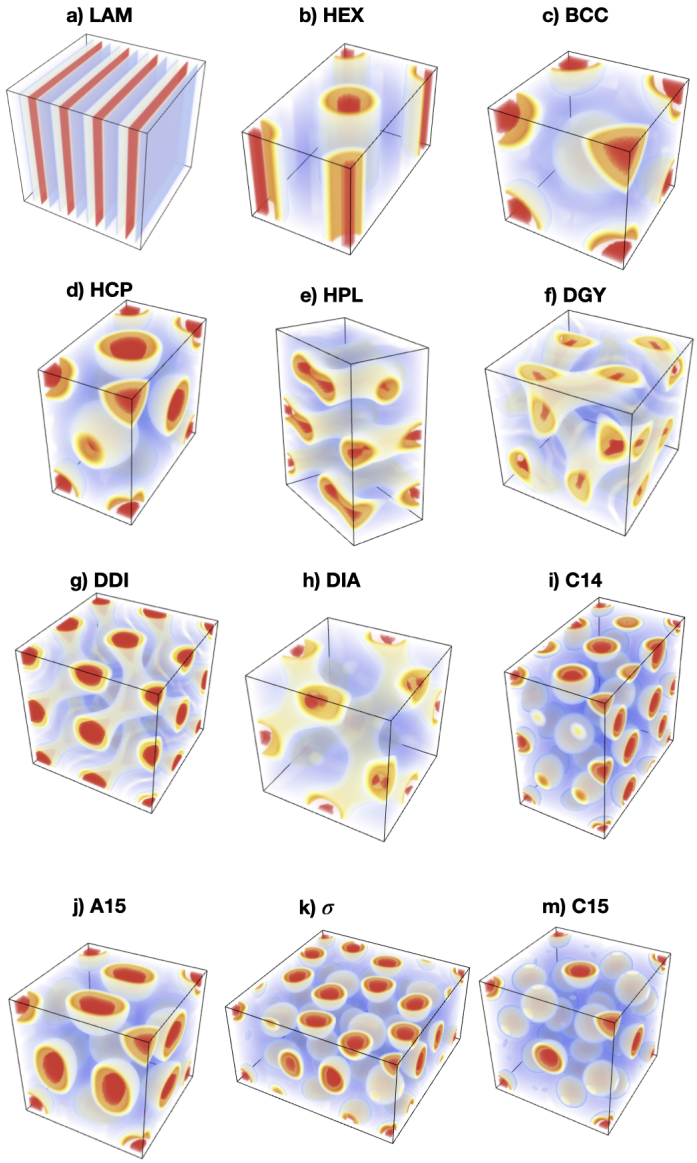

Figure 2.3: Monomer density profiles of the candidate phases and their abbreviations. a) Lamellar (LAM) b) Hexagonal cylinders (HEX) c) Body-centred cubic (BCC) d) Hexagonal close-packed spheres (HCP) e) Hexagonally-perforated lamellar (HPL) f) double gyroid (DGY) g) double diamond (DDI) h) diamond (DIA) i) C14 j) A15 m) σ k)C15

Chapter 3

Results: A-c-B Type Polymers

In this chapter, we explore the sensitivity of the phase behaviour of AB diblock copolymers to the addition of a single C-monomer at the AB junction. We also explore the effects of changing the characteristics of the C-monomer. To better understand the sensitivity of the phase behaviour, we compare the results to the phase diagram of an AB diblock copolymer melt with $N_A = 12$, as shown in Fig. 3.1. Note, there is a small area where BCC is stable near the ODT; however, since it is so small is not labelled but is shown in Fig. 3.2. It is also of note that all of the ODT and sometimes the BCC->HEX phase boundaries have a significantly larger error than the others plotted due to the inability to converge ordered phases past the ODT.

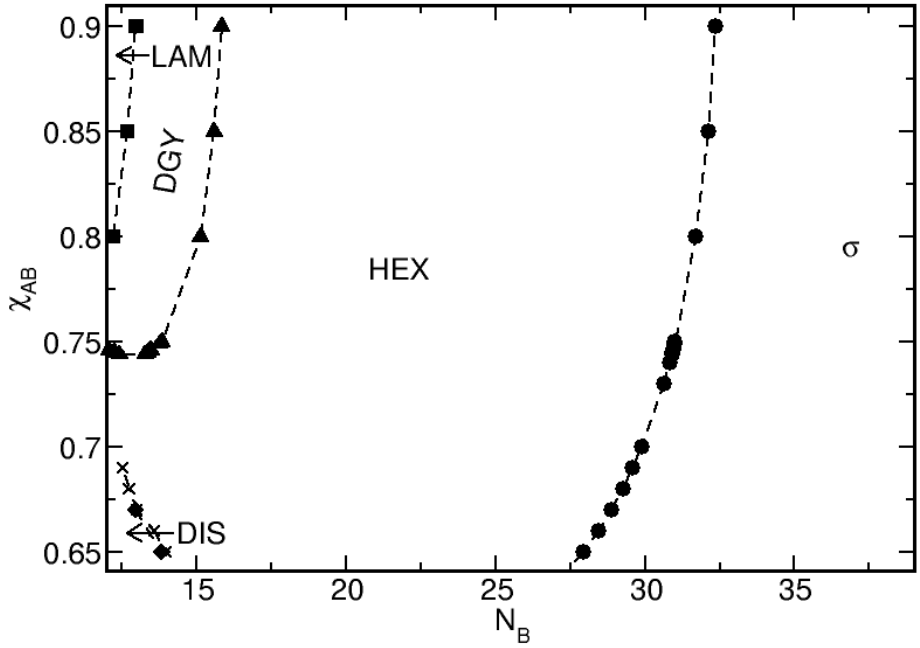

FIGURE 3.1: Reference phase diagram in the $\chi_{AB} - N_B$ plane for AB block copolymers, with N_A=12 and $b_B = 0.5b_A$.

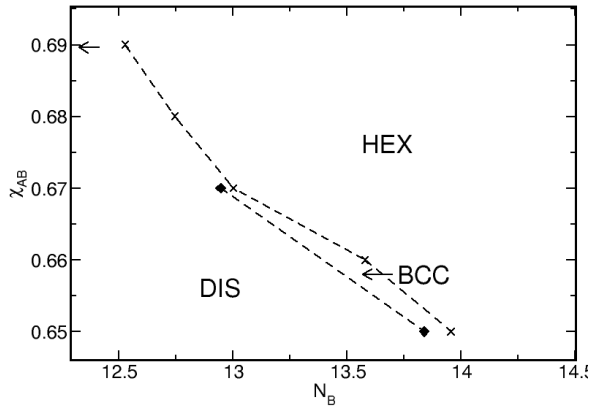

FIGURE 3.2: Phase boundaries near the ODT for AB diblock copolymers, with N_A=12.

Upon first glance, the results in Fig. 3.1, may not appear to be the same as the results in Fig. 1.6. There are a few reasons for these observed differences. The first is that the conformational asymmetry is different. In the SCFT results in Fig. 1.6, block copolymers with $b_A/b_B = 1$ are used, while here $b_A/b_B = 2$. The phase diagram in Fig. 1.6 also does not contain the σ phase, because it had not yet been discovered and therefore would not have been considered a candidate phase. Finally, the phase diagrams are plotted in different planes. In Fig 1.6, the phase diagram is plotted in the $\chi_{AB}N$-f_A plane, while in Fig. 3.1, the phase diagram is plotted in the $\chi_{AB} - N_B$ plane. In Fig. 3.3 c), we replot the phase diagram from Fig. 3.1 in the $\chi_{AB} - f_A$ plane, with the red outline indicating the area for which we obtained results. In Fig. 3.3 a), we show a phase diagram for diblock copolymers with $b_A/b_B = 2$ from Ref. [58]. We note that this study did not consider the presence of the σ phase, so the

only phase boundaries that should be compared to the results in Fig. 3.3 c) are those that are between phases with non-spherical micelles. In Fig. 3.3 b), a phase diagram containing the phases with spherical micelles for diblock copolymers from Ref [59] is displayed. By comparing a) and b) to c), we can see that the results are consistent.

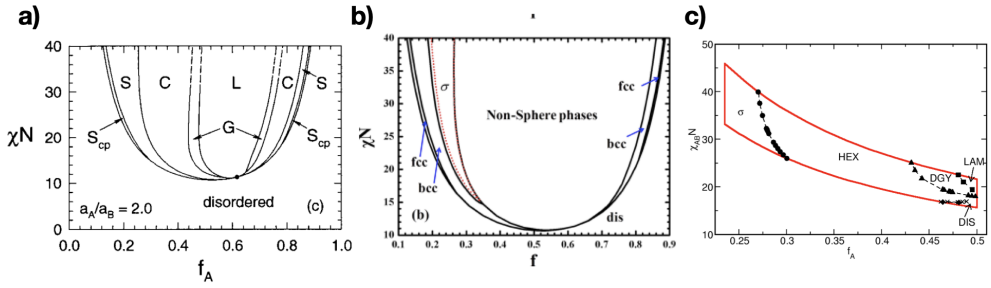

FIGURE 3.3: Phase diagram comparison with known results for $b_A/b_B = 2$ from a) [58], b) [59], and c) Fig. 3.1. The labelling of the phases are as follows: L=LAM, G=DGY, C=HEX, S=bcc=BCC, $S_{cp} = HCP$, fcc=Face-centred cubic, and disordered=dis=DIS. Further $f = f_A$ and $\chi = \chi_{AB}$. Figures reproduced with permission of publisher.

3.1 A-c-B Results

We first present the results for the various A-c-B scenarios examined. The first case adds a C-monomer that is either nearly-neutral or neutral, and it interacts with the A and B blocks in the same manner, $\chi_{AC} = \chi_{BC}$. The resultant phase diagram is shown in Fig. 3.4.

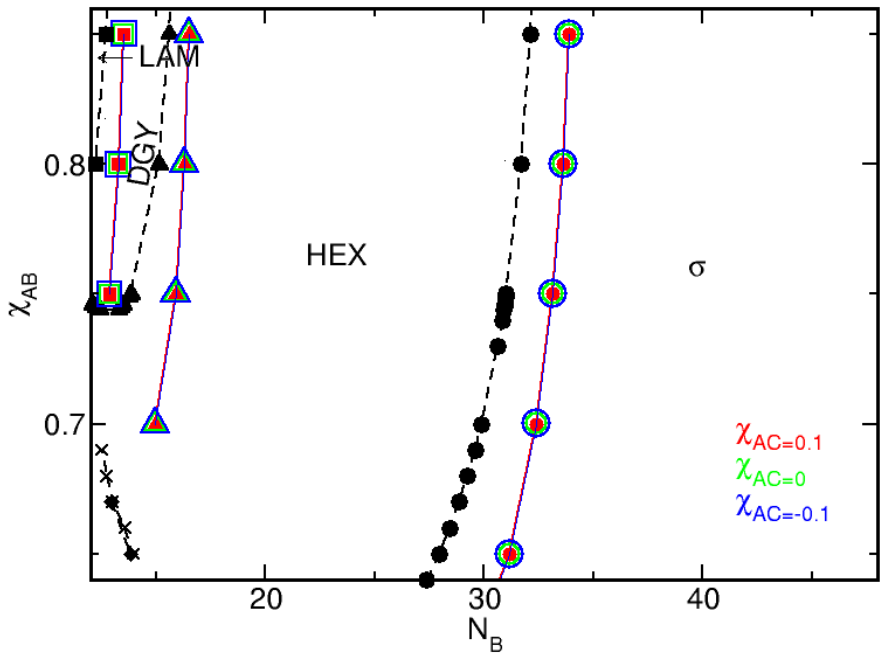

FIGURE 3.4: Phase diagram in the $\chi_{AB} - N_B$ plane for A-c-B block copolymers, with N_A=12. The interactions with the C-monomer are such that $\chi_{AC} = \chi_{BC} = -0.1, 0, 0.1$. The Ds with the dashed lines are the equivalent phase boundaries for an AB diblock copolymer melt with N_A=12.

The main notable feature is the marked shift of all phase boundaries to larger values of N_B and lower values of χ_{AB} than the corresponding phase boundaries of the AB diblock copolymers. Upon closer inspection of the phase boundaries, we note that they do not perfectly overlap, but rather are slightly shifted with respect to each other, as shown in Fig. 3.5. If we first examine the DGY to HEX and LAM to DGY boundaries (triangles and squares, respectively), we see that as $\chi_{AC} = \chi_{BC}$ decreases,

the boundaries are increasingly shifted to the higher values of N_B. In contrast, the HEX to σ boundary (circles) exhibits the opposite effect, but overall this is a very small effect.

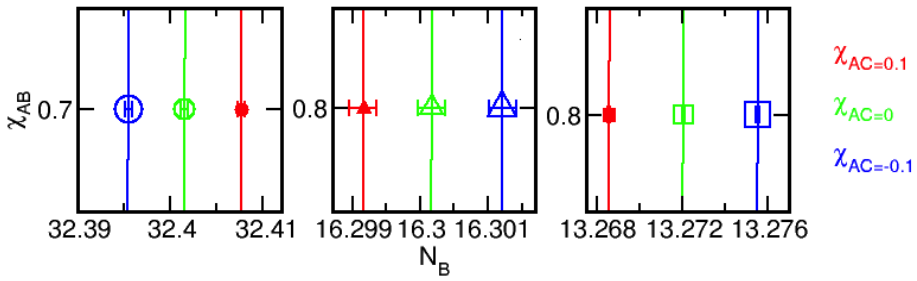

FIGURE 3.5: Closer view of phase boundaries for diblock copolymers with a nearly-neutral C-monomer added to the junction. Results are shown for the HEX to σ (circles) junction for χ_{AB}=0.7 and the DGY to HEX (triangles) and LAM to DGY (squares) boundaries at χ_{AB}=0.8.

While the previous model showed that the C-monomer does have an effect, the choice of χ_{AC} and χ_{BC} is not likely to be a good model of what could be seen experimentally since the interactions between monomers of types i and j can be expressed as [2],

$$\chi_{ij} = C_{1,ij} + \frac{C_{2,ij}}{T}, \tag{3.1}$$

where $C_{1,ij}$ and $C_{2,ij}$ are constants that that depend on the monomer species and T is temperature. Thus changing χ_{AB} without changing monomer species means changing T. It is therefore more reasonable to expect χ_{AC} and χ_{BC} to depend on temperature. In a very broad sense, we have 4 independent parameters related to the C-monomer that can be change independently: $C_{1,AC}$, $C_{2,AC}$, $C_{1,BC}$, and $C_{2,BC}$. However, in this

thesis, we choose a simplified model where χ_{AC} and χ_{BC} are given by,

$$\chi_{\mathrm{AC}} = \chi_{\mathrm{AB}} + \alpha, \tag{3.2}$$

$$\chi_{\mathrm{BC}} = \chi_{\mathrm{AB}} - \alpha, \tag{3.3}$$

where α is constant. In employing this model, we are effectively setting the $C_{2,\mathrm{AC}} = C_{2,\mathrm{BC}} = C_{2,\mathrm{AB}}$ and defining $\alpha \equiv \chi_{\mathrm{AC}} - \chi_{\mathrm{AB}} = C_{1,AC} - C_{1,AB}$. The resultant phase diagrams, plotted in two different ways, for various values of α are shown in Figs. 3.6 and 3.7.

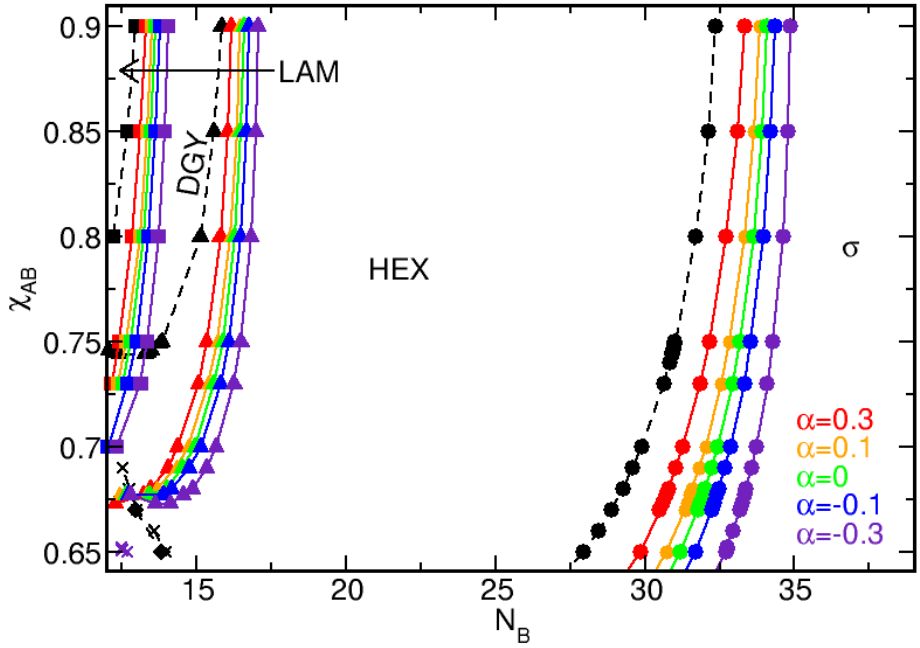

FIGURE 3.6: Phase diagram in the $\chi_{AB} - N_B$ plane for diblock copolymers with a C-monomer added to the junction where $\chi_{AC} = \chi_{AB} + \alpha$ and $\chi_{BC} = \chi_{AB} - \alpha$. Results are overlaid for $\alpha = \pm 0.3,\ \pm 0.1,\ 0$. The dashed lines are the same as in Fig. 3.4. Not that some areas are not labelled near the ODT.

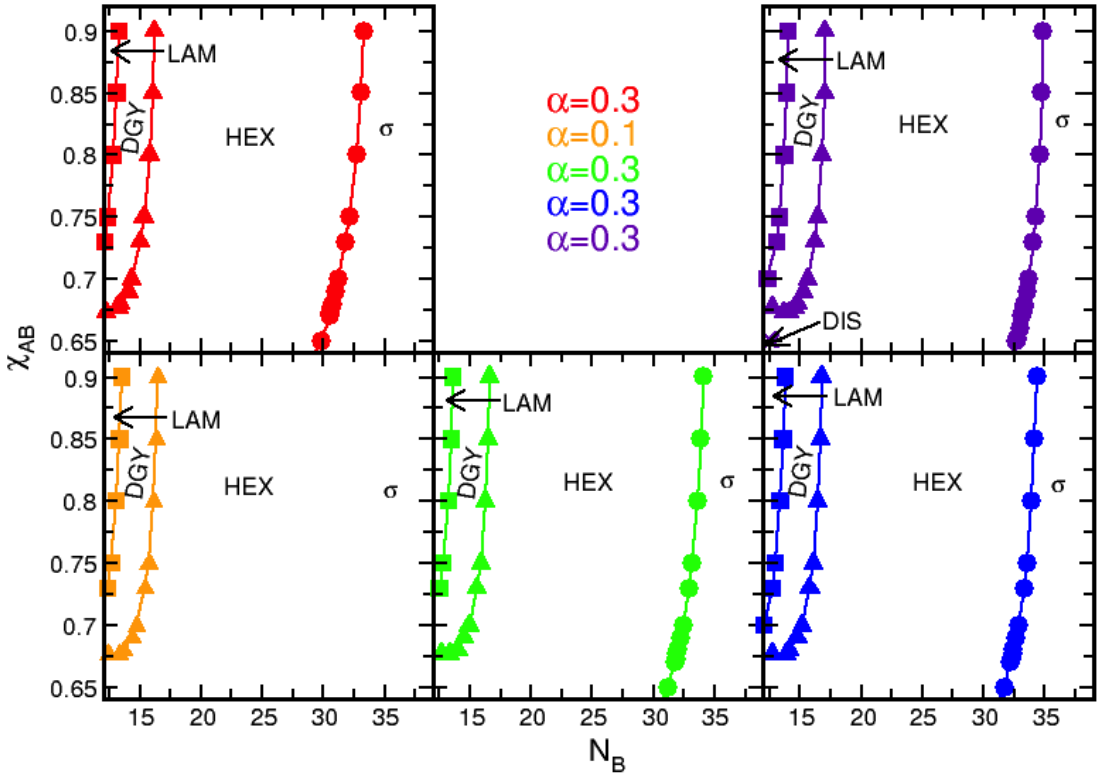

FIGURE 3.7: The same phase diagrams as in Fig. 3.6, except now the various values of α are plotted separately

In Figs. 3.6 and 3.7, we again notice a shift of all phase boundaries to larger values of N_B and smaller χ_{AB}. The various values of α also display different sized shifts with the largest value of α displaying the smallest shifts.

Finally, in chapter 2, it was stated that monomers of type i and j interact with each other through the finite-range interaction given in Eq. 2.8, where σ_{ij} gives a measure of the distance over which the monomers feel this interaction. In all of the

other results of this thesis, we take $\sigma_{AB} = \sigma_{AC} = \sigma_{BC} = \sqrt{3}$, or defining δ as

$$\delta_{FR} = \frac{\sigma_{AC}}{\sigma_{AB}} = \frac{\sigma_{BC}}{\sigma_{AB}}, \tag{3.4}$$

we have $\delta_{FR} = 1$. However, we also examine the effects of changing δ_{FR}. The results are shown in Fig. 3.8 for $\chi_{AB} = \chi_{AC} = \chi_{BC}$, or $\alpha = 0$.

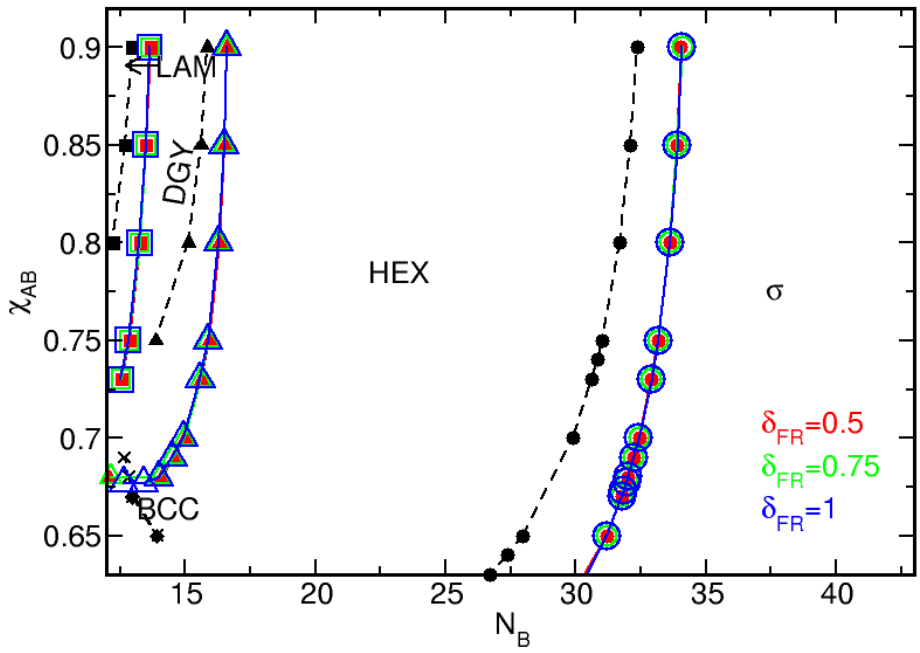

FIGURE 3.8: Phase diagram in the $\chi_{AB} - N_B$ plane for diblock copolymers with a C-monomer added to the junction where $\chi_{AC} = \chi_{AB} + \alpha$ and $\chi_{BC} = \chi_{AB} - \alpha$ and the $\sigma_{AC} = \sigma_{BC} \neq \sigma_{AB}$. Results are shown for $\sigma_{AC} = \sigma_{BC} = 0.5\sigma_{AB}$ and$\sigma_{AC} = \sigma_{BC} = 0.75\sigma_{AB}$. The dashed lines are the same as in Fig. 3.4.

Once again, we note the same type of shift of all phase boundaries to larger N_B and smaller χ_{AB}. If we take a closer look, as displayed in Fig. 3.9, we can see that both δ_{FR} =0.5 and 0.75 are slightly shifted from $\delta_{FR} = 1$, with $\delta = 0.5$ having the largest shift. It is also interesting to note that the direction of the shift is to larger values of N_B for the LAM to DGY (squares) and DGY (triangles) to HEX boundaries and to smaller values N_B for the HEX to SIG (circles) boundary. This effect however is very small.

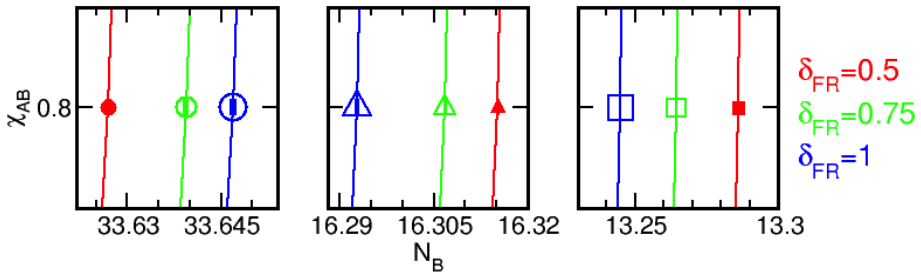

FIGURE 3.9: Closer view of phase boundaries for diblock copolymers with a C-monomer added to the junction where χ_{AC} and χ_{BC} are temperature dependent and the $\sigma_{AC} = \sigma_{BC} \neq \sigma_{AB}$ for the HEX to σ (circles), DGY to HEX (triangles), and LAM to DGY (squares) boundaries at χ_{AB}=0.8

3.2 Discussion

The main result from the above phase diagrams is that the addition of a single C-monomer to the junction of the AB diblock copolymers does have a noticeable effect on the phase boundaries. However, since the effect is simply a shift, the phases that are present and the sequence of the phase transitions remains unchanged. In order to

understand the roots of this behaviour, we consider two important factors that play a role in determining the position of the phase transitions: the interfacial tension and the polymer stretching energy.

The first factor to consider is the polymer stretching energy. To evaluate the effects of the C-monomer on the polymer stretching, we examine the domain size, L_x, of the HEX phase as shown in Fig. 3.10. In Table 3.1, results for L_x are shown for the various scenarios investigated here and for the AB diblock copolymers as a reference. The results display a notable increase in the domain size of the A-c-B type copolymer melts from that of the AB copolymer melts. While, we would expect a slight increase due to the polymer now being slightly longer, this would leave the ratio of L_x to the average size of the polymer to remain the same. To check this, we take the size of the polymer to be given by the root-mean-square end-to end distance:

$$R_{ee} = \sqrt{\sum_{i=1}^{N-1} b_i^2} = \begin{cases} \sqrt{19}, & \text{A-c-B} \\ \sqrt{18}, & \text{AB} \end{cases} \tag{3.5}$$

where i labels bond and the numerical results are for $N_B = 25$. As displayed in Table 3.10, there is an increase in the domain size that is not accounted for by just the increase in polymer length. These results indicate increased chain stretching due to the presence of the C-monomer. This increased chain stretching causes the melt to prefer phases that decrease this stretching, or the less spherical phases.

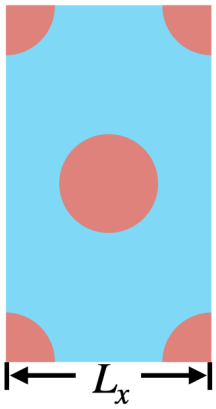

FIGURE 3.10: Illustration of L_{x} for hexagonal-packed cylinders

AB diblock	10.5853	2.4950
$\chi_{AC} = \chi_{BC}$	L_x	L_x/R_{ee}
0.1	11.0839	2.5428
0	11.0815	2.5423
-0.1	11.0793	2.5418
α	L_x	L_x/R_{ee}
0.3	11.1060	2.5479
0.1	11.1015	2.5469
0	11.0990	2.5463
-0.1	11.0964	2.5457
-0.3	11.0908	2.5444
δ	L_x	L_x/R_{ee}
1	11.0990	2.5463
0.75	11.1011	2.5468
0.5	11.1022	2.5470

TABLE 3.1: L_x for hexagonal-packed cylinders for the various A-c-B block copolymers examined with $\chi_{AB} = 0.75$ and $N_B = 25$.

The other factor to consider is the interfacial tension. While this is not straightforward to calculate, we can get a measure of the apparent interfacial tension by following the procedure set out in Ref. [82]. In this paper, Shi and Noolandi showed that the interfacial tension of the diblock copolymer blends can be estimated by fitting the low

L_x part of the free energy curves to a γ/L_x function and then taking γ as an estimate of the interfacial tension. Example curves and fits are shown in Fig. 3.11. Using this method, we find the resultant apparent interfacial tensions that are displayed in Table. 3.2. We see an increase in the γ in all cases, which would result in the phase boundaries moving to lower values of N_B and lower values of χ_{AB}.

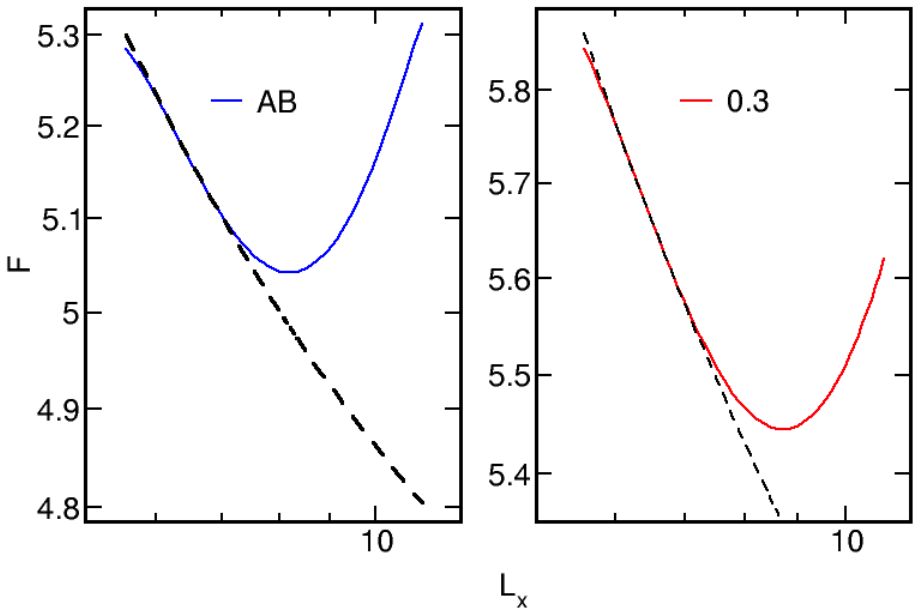

FIGURE 3.11: Plot of the free energy of the lamellar phase vs domain spacing for AB diblock copolymers on the left and A-c-B polymers with $\alpha = 0.3$ on the right. In both plots $\chi_{AB} = 0.85$ and $N_B = 13$ The black dashed lines are fits to A/L_x+B.

System	$\gamma \pm 0.2$
AB diblock	5.6
$\chi_{AC} = \chi_{BC}$	
0.1	7.7
0	7.7
-0.1	7.7
α	
0.3	8.0
0.1	7.8
0	7.7
-0.1	7.5
-0.3	7.4
δ	
1	7.7
0.75	7.7
0.5	7.8

TABLE 3.2: γ for lamallae for the various A-c-B block copolymers examined with $\chi_{AB} = 0.85$ and $N_B = 13$.

Combining these effects, we understand the shifts as follows. The increased stretching energy due to the increased domain size accounts for the main generic shift to larger values of N_B. On the other hand, the increased apparent interfacial tension

accounts for the shift to lower values of χ_{AB}.

Looking at the more detailed effects of changing the properties of the monomers, the difference in shift due to changing χ_{AC} and χ_{BC} in the case of the nearly-neutral C-monomers or of changing the range of the finite-range interaction is very small and in normal phase diagram is not visible. Therefore, we conclude that these two changes do not have any visible effect on the shift.

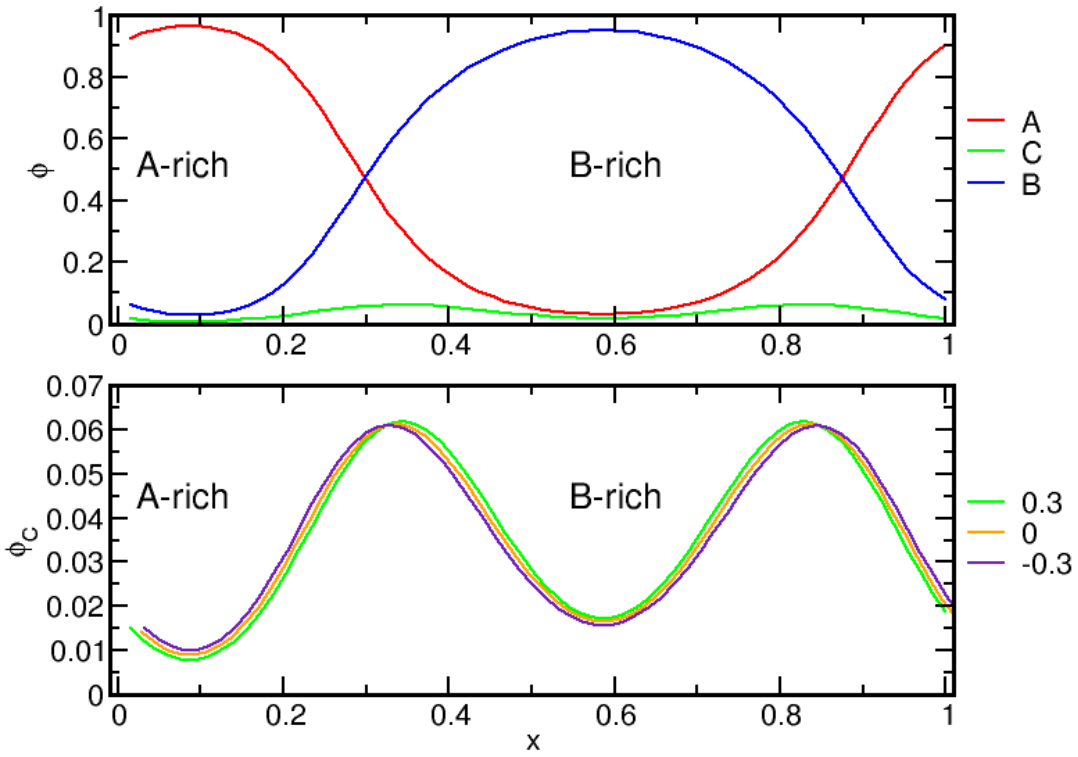

FIGURE 3.12: Lamellar density profiles for A-c-B melts with $\chi_{AB} = 0.75$ and $N_B = 15$. Top: Monomer density profiles for A, B and c monomers with $\alpha = 0.3$. Bottom: C-monomer density profiles for various $\alpha = \pm 0.3$ and 0

α	$L_{x,A}/d$
0.3	0.4233
0.1	0.4244
0	0.4249
-0.1	0.4254
-0.3	0.4264

TABLE 3.3: $L_{x,A}$ for lamellar for A-c-B block copolymers with $\chi_{AB} = 0.85$ and $N_B = 13$ for varying α

Conversely the shift is strongly dependant on α. More specifically, we note that larger values of α lead to smaller shifts. To understand this we examine the density profiles of the lamellar phase as plotted in Fig. 3.12. We also simultaneously consider the A-rich domain size, $L_{x,A}/d$ which is displayed in Table 3.3 which is calculated by taking the points where $\phi_A = \phi_B$ as the boundaries between the two domains. In the lower plot of Fig. 3.12 notice that as α decreases, the distribution of the C-monomers favours the A-rich region. This behaviour is expected given the definition of χ_{AC} and χ_{BC} and has the effect of effectively increasing the size of the A-rich region. The second thing to note, is that by examining the apparent interfacial tension, we see that while changing $\chi_{AC} = \chi_{BC}$ or the finite-range interaction range does not change γ significantly, changing α has a noticeable effect on the interfacial tension suggesting that the change in γ is associated with the change in shift size due to changing α. Therefore, we conclude that the increase in the A-rich domain size

together with decrease in interfacial tension as α decreases causes the melts with the smallest α to more strongly favour the less spherical configurations and have a larger shift, consistent with Fig. 3.6.

Chapter 4

Results: A-B-c Type Polymers

4.1 Results

We now examine the effect of placing a C-monomer at the free end of the majority block. The C-monomer will be modelled as having the same finite-range interaction range as the A and B monomers and with χ_{AC} and χ_{BC} given by Eqs. 3.2 and 3.3, respectively. The results are shown in Figs. 4.1 and 4.2.

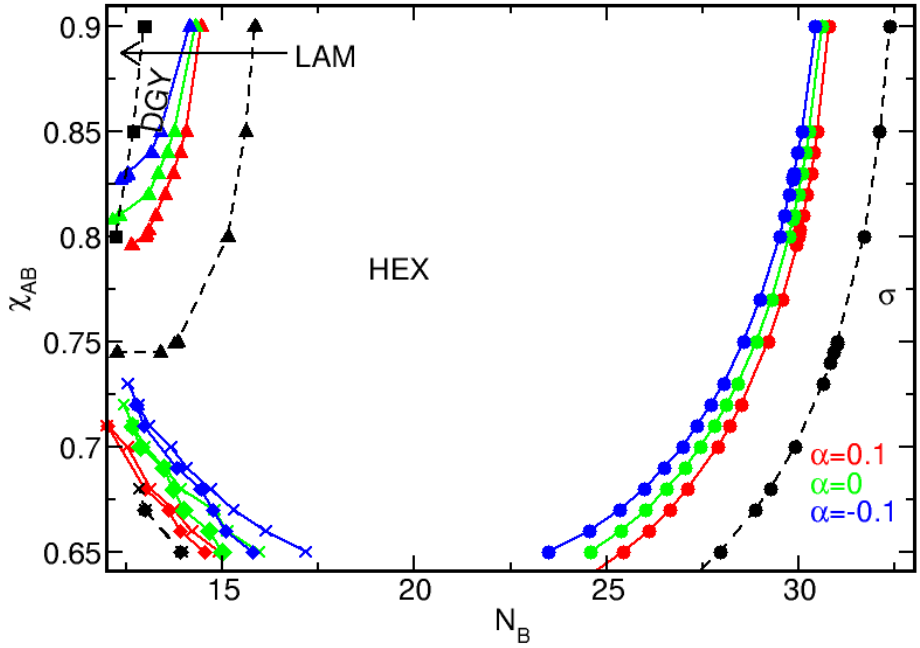

FIGURE 4.1: Overlaid phase diagram in the $\chi_{AB}-N_B$ plane for diblock copolymers with a C-monomer added to the majority end where $\chi_{AC} = \chi_{AB} + \alpha$ and $\chi_{BC} = \chi_{AB} - \alpha$. Results are shown for $\alpha = \pm 0.1,$ and 0. The dashed lines are the same as in Fig. 3.4. Note, some areas in the phase diagram are not labelled.

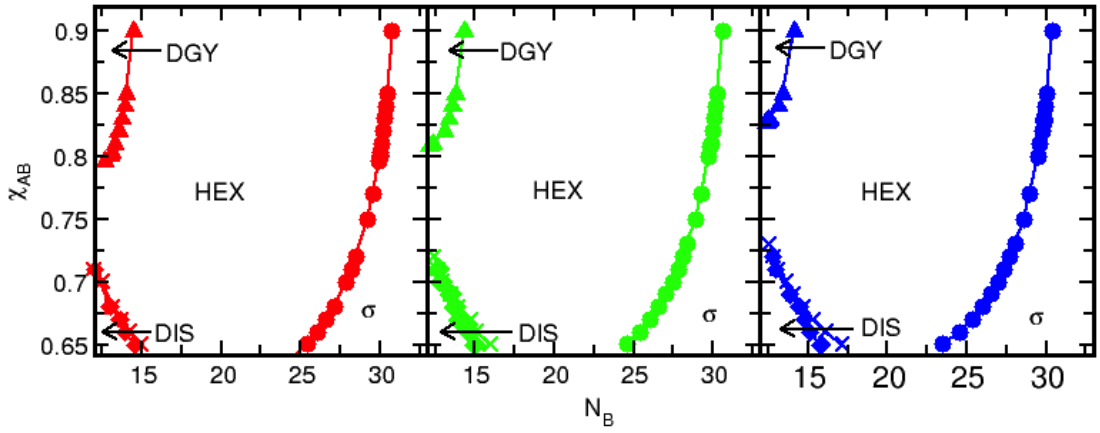

FIGURE 4.2: The same phase diagrams as in Fig. 4.1, except now the various values of α are plotted separately

Looking at Figs. 4.1 and 4.2, we see two notable features. First, there is a notable shift in the phase boundaries to lower values of N_{B} and higher values of χ_{AB} when compared to the AB diblock copolymer phase boundaries.We further note that the shift size varies with α with the smallest α having the largest shift.

4.2 Discussion

Once again, we examine two main properties to help elucidate the physics behind the shift. The first important factor is the polymer stretching energy. Table 4.1 shows the domain sizes for the various values of α. We see that there is a notable decrease in both L_{x} and $L_{\mathrm{x}}/R_{\mathrm{ee}}$ when compared to the diblock copolymer domain size. This decrease means that the polymers are stretched less and therefore the melt can transition to more spherical phases at smaller values of N_{B}.

α	L_x	L_x/R_{ee}
0.1	10.5133	2.4119
0	10.4563	2.3988
-0.1	10.4563	2.3854
AB diblock	10.5853	2.4950

TABLE 4.1: L_x for hexagonal-packed cylinders for A-B-c block copolymers with $\chi_{AB} = 0.75$ and $N_B = 25$ for various values of α

The other main important factor to consider is the interfacial tension. By measuring the apparent interfacial tension in an identical manner to what was done in Ch. 3, we obtain the results displayed in Table. 4.2. There is a notable decrease in the apparent interfacial tension from that of the AB diblock melt. We also note that the decrease is most significant for the lowest value of α

System	$\gamma \pm 0.2$
AB diblock	5.6
α	
0.1	4.8
0	4.3
-0.1	3.9

TABLE 4.2: γ for lamallae for the various A-B-c block copolymers examined with $\chi_{AB} = 0.85$ and $N_B = 13$.

Finally, we consider the size of the A-rich domain, as displayed in Table. 4.3, we see the opposite trend to what we expect. When the domain size of the A-rich region is largest, the boundaries are at the smallest N_{B}. However, in this system, the change in the size of the A-domain is small compared to the change in the total domain size, and therefore, we do not expect the this change to play a large role in determining the shift size.

α	$L_{\mathrm{x,A}}/d$
0.1	0.4150
0	0.4155
-0.1	0.4159

TABLE 4.3: $L_{\mathrm{x,A}}$ for lamellar for A-B-c block copolymers with $\chi_{\mathrm{AB}} = 0.75$ and $N_{\mathrm{B}} = 15$ for various values of α

Combining these results, we see that the large changes noted in the apparent interfacial tension and in the polymer stretching will dominate the results, while the change in the A-domain size is small and therefore will not play a large role. Further, we see that the decrease in polymer stretching causes the main shift to lower values of N_{B}. Further, the significant decrease in the γ will cause the shift to larger χ_{AB}. Further, since the magnitude of the change in γ is dependant on α with the smallest α displaying the largest change, the shift for smallest α will be the largest, consistent with Figs. 4.1 and 4.2.

Chapter 5

Conclusions

In this study, we have examined the sensitivity of the phase behaviour of AB diblock copolymers to the addition of a single C-monomer. To accomplish this, we model the polymers as short freely-jointed chains with an A-block length of $N_{\mathrm{A}} = 12$. We then employ self-consistent mean-field theory (SCFT) to construct phase diagrams which are compared to the phase diagrams of comparable AB diblock copolymers.

The first scenario examined adds various types of C-monomers to the junction of the AB diblock, thus making A-c-B type block copolymers. In all cases examined, one of the most notable effects is a shift of all phase boundaries to larger values of N_{B} and lower values of χ_{AB} than that of the AB diblock copolymers. Upon examination, we find that the domain size increases in all cases for A-c-B type copolymers with little variation among the different types of C-monomers. This increase will increase the stretching of the polymers and will cause the shift in phase boundaries to larger values of N_{B}. Further, we find an increase in the apparent interfacial tension that causes

the phase boundaries to shift to lower χ_{AB}. We also examined the sensitivities of the phase boundaries to the properties of the C-monomers. One of the cases examines adding nearly-neutral C-monomers, where $\chi_{AC} = \chi_{BC}$ and both are close to zero and do not depend on temperature. In this case, the value of $\chi_{AC} = \chi_{BC}$ did not visibly change in the size of the shift. When examining the effects of changing the range of the finite-range interaction between different monomer species, this also was found to not have a significant effect on the size of the shift. However, when examining the case where $\chi_{AC} = \chi_{AB} + \alpha$ and $\chi_{BC} = \chi_{AB} - \alpha$, α was found to to significantly effect the size of the observed shift with larger αs exhibiting a larger shift. This variation is due to an increase in the A-rich domain size that increased with decreasing α and the interfacial tension further increasing as α increased.

The next scenario that was examined adds the C-monomer to the majority end of the AB diblock copolymer. The C-monomers added are characterised by $\chi_{AC} = \chi_{AB} + \alpha$ and $\chi_{BC} = \chi_{AB} - \alpha$. Due to this addition, all phase boundaries were shifted to the lower N_B and larger χ_{AB} when compared to those of the AB diblock copolymers. Examination of the domain size shows a decrease in domain size when the C-monomer is present, thus decreasing the stretching energy and causing the general observed shift to smaller N_b. The apparent interfacial tension was also found to decrease with the smallest α displaying the largest decrease, causing the shift of the phase boundaries to larger χ_{AB}. Further, the size of both the horizontal and vertical shift depends α, with the smallest α having the largest shift. Closer examination of the domain sizes reveals that the decrease in domain size is largest for the smallest value of α, and

that there is very little variance in the A-rich domain size. Thus, the combination of the domain size variation and the variation in the apparent interfacial tension with α leads to the observed variation in shift size.

The motivation of this project is to provide a link between experiments, which often have the C-monomers, and theoretical techniques, which often do not examine the sensitivity of the phase behaviour to the addition of a single C-monomer theoretically. This area of research is important because several experimental techniques, such as the click-method, have these single C-monomers at either the junction or the ends and experimentally these single monomers have shown promise to be used in tuning the phase behaviour of block copolymers melts. In this study we were able to show that while an observable difference is seen in the position of the phase boundaries, the main sequence was not affected.

There is still much to explore in this area to further understand the effects of having a C-monomer added to AB diblock copolymers. One very closely related project would be to examine c-A-B type polymers. A further interesting project would be to examine how strong this effect is in longer polymers, since the ones used in this study were rather short, with $N_{\mathrm{A}} = 12$. Further the cases considered here are fairly simple cases to start to explore their effects, however exploring more complex cases or other types of C-monomers could yield interesting results. One interesting point would be to examine the effects on adding a C-monomer on both ends, or one at the centre along with one at either one or both ends. Another area that could

be examined is changing the temperature-dependence of the interactions with the C-monomers. Adding in electrostatic interactions could also prove very useful as many of the experiment studies examining these types of systems also include electrostatics.

Appendix A

Mixing Methods

In this section we briefly describe the mixing methods that are used in the program.

A1 Simple Mixing

The first method that is used is simple mixing. In simple mixing the chemical potential fields are updated using:

$$\omega_{\mathrm{A}}^{\mathrm{new}}(\vec{r}) = \omega_{\mathrm{A}}(\vec{r}) + \lambda^{\mathrm{SM}} d\omega_{\mathrm{A}}(\vec{r}), \tag{A.1}$$

$$\omega_{\mathrm{B}}^{\mathrm{new}}(\vec{r}) = \omega_{\mathrm{B}}(\vec{r}) + \lambda^{\mathrm{SM}} d\omega_{\mathrm{B}}(\vec{r}), \tag{A.2}$$

and

$$\omega_{\mathrm{C}}^{\mathrm{new}}(\vec{r}) = \omega_{\mathrm{C}}(\vec{r}) + \lambda^{\mathrm{SM}} d\omega_{\mathrm{C}}(\vec{r}) \tag{A.3}$$

where λ^{SM} is a numerical factor chosen to be 0.05. Further, since we allow for variable box dimensions, the box parameters are similarly updated by

$$\theta_{box}^{\mathrm{new}} = \theta_{\mathrm{box}} + \lambda^{\mathrm{SM}} d\theta_{\mathrm{box}}(\vec{r}) \tag{A.4}$$

A2 Anderson Mixing

As seen in the previous section, simple mixing uses the input of residuals from only a single time step back. While this method works, it may be time consuming to reached the desired accuracy. Therefore, after we have used simple mixing to ensure that we have a good history of residuals and fields, we employ variable-cell Anderson mixing, which uses the optimal combination of residuals from n_{And} previous iterations. While a general derivation is not given here, it can be found in Refs [11, 78, 83].

We first define the matrix $\mathbf{U}$ with elements given by,

$$\begin{aligned} U_{mn} = &\langle d\omega_{A,i} - d\omega_{A,i-n} | d\omega_{A,i} - d\omega_{A,i-m} \rangle \\ &+ \langle d\omega_{B,i} - d\omega_{B,i-n} | d\omega_{B,i} - d\omega_{B,i-m} \rangle \\ &+ \langle d\omega_{C,i} - d\omega_{C,i-n} | d\omega_{C,i} - d\omega_{C,i-m} \rangle \\ &+ \langle d\theta_{box,x,i} - d\theta_{box,x,i-n} | d\theta_{box,x,i} - d\theta_{box,x,i-m} \rangle \\ &+ \langle d\theta_{box,y,i} - d\theta_{box,y,i-n} | d\theta_{box,y,i} - d\theta_{box,y,i-m} \rangle \\ &+ \langle d\theta_{box,z,i} - d\theta_{box,z,i-n} | d\theta_{box,z,i} - d\theta_{box,z,i-m} \rangle, \end{aligned} \tag{A.5}$$

where we use the convention,

$$\langle f|g\rangle = \begin{cases} \int f(\vec{r})g(\vec{r})d\vec{r}, & when\ f = f(\vec{r})\ and\ g = g(\vec{r}) \\ f * g, & otherwise. \end{cases} \tag{A.6}$$

and the subcripts i, $i-n$, and $i-m$ indicate the residuals are from the ith, $i-n$th and $i-m$th interation. Then, we define the matrix $\mathbf{V}$ with matrix elements,

$$\begin{aligned} V_n = &\langle d\omega_{A,i} - d\omega_{A,i-n}|d\omega_{A,i}\rangle \\ &+ \langle d\omega_{B,i} - d\omega_{B,i-n}|d\omega_{B,i}\rangle \\ &+ \langle d\omega_{C,i} - d\omega_{C,i-n}|d\omega_{C,i}\rangle \\ &+ \langle d\theta_{box,x,i} - d\theta_{box,x,i-n}|d\theta_{box,x,i}\rangle \\ &+ \langle d\theta_{box,y,i} - d\theta_{box,y,i-n}|d\theta_{box,y,i}\rangle \\ &+ \langle d\theta_{box,z,i} - d\theta_{box,z,i-n}|d\theta_{box,z,i}\rangle, \end{aligned} \tag{A.7}$$

Using these we obtain the matrix $\mathbf{A}$

$$A_n = U^{-}_{nm} 1 V_m \tag{A.8}$$

And, the chemical potential fields are then updated by,

$$\omega_{A,i+1}(\vec{r}) = \omega^{new}_{A}(\vec{r}) + \sum_n A_n(\omega^{new}_{A,i-n}(\vec{r}) - \omega^{new}_{A,i}(\vec{r})) \tag{A.9}$$

$$\omega_{B,i+1}(\vec{r}) = \omega_B^{new}(\vec{r}) + \sum_n A_n(\omega_{B,i-n}^{new}(\vec{r}) - \omega_{B,i}^{new}(\vec{r})) \tag{A.10}$$

$$\omega_{C,i+1}(\vec{r}) = \omega_C^{new}(\vec{r}) + \sum_n A_n(\omega_{C,i-n}^{new}(\vec{r}) - \omega_{C,i}^{new}(\vec{r})) \tag{A.11}$$

and the box widths are updated by,

$$\theta_{box,x,i+1} = \theta_{box,x}^{new} + \sum_n A_n(\theta_{box,x,i-n}^{new} - \theta_{box,x,i}^{new}), \tag{A.12}$$

$$\theta_{box,y,i+1} = \theta_{box,y}^{new} + \sum_n A_n(\theta_{box,y,i-n}^{new} - \theta_{box,y,i}^{new}), \tag{A.13}$$

$$\theta_{box,z,i+1} = \theta_{box,z}^{new} + \sum_n A_n(\theta_{box,z,i-n}^{new} - \theta_{box,z,i}^{new}), \tag{A.14}$$

where θ_{box}^{new} is as in Eq. A.4 with $\lambda_{\mathrm{SM}} = 1$.

Bibliography

[1]A. S. Abd-El-Aziz, M. Antonietti, C. Barner-Kowollik, W. H. Binder, A. Böker, C. Boyer, M. R. Buchmeiser, S. Z. Cheng, F. D'Agosto, G. Floudas, et al., The next 100 years of polymer science, *Macromolecular Chemistry and Physics* **221**(16), 2000216 (2020).

[2]M. Rubinstein and R. H. Colby, *Polymer Physics*, Oxford University Press, Oxford, 2003.

[3]H. Namazi, Polymers in our daily life, *BioImpacts: BI* **7**(2), 73 (2017).

[4]V. Wong, Inspirational chemistry: resources for modern curricula, (2006).

[5]*Editors of encyclopedia britannica, polymer summary, encyclopedia britannica,* ***2020****. https://www.britannica.com/summary/polymer.*

[6]A.-C. Shi, Frustration in block copolymer assemblies, *Journal of Physics: Condensed Matter* **33**(25), 253001 (2021).

[7]L. Gerrits, R. Hammink, and P. H. Kouwer, Semiflexible polymer scaffolds: an overview of conjugation strategies, *Polymer Chemistry* **12**(10), 1362–1392 (2021).

[8]H. Dau, G. R. Jones, E. Tsogtgerel, D. Nguyen, A. Keyes, Y.-S. Liu, H. Rauf, E. Ordonez, V. Puchelle, H. Basbug Alhan, et al., Linear block copolymer synthesis, *Chemical Reviews* **122**(18), 14471–14553 (2022).

[9]E. Chernikova and Y. Kudryavtsev, RAFT-based polymers for click reactions, *Polymers* **14**, 570 (2022).

[10]H. Feng, X. Lu, W. Wang, N.-G. Kang, and J. W. Mays, Block copolymers: synthesis, self-assembly, and applications, *Polymers* **9**(10), 494 (2017).

[11]C. T. Lai, Theory of disperse diblock copolymers, PhD. thesis (McMaster University, 2022).

[12]M. W. Matsen and F. S. Bates, Origins of complex self-assembly in block copolymers, *Macromolecules* **29**(23), 7641–7644 (1996).

[13]A. K. Khandpur, S. Foerster, F. S. Bates, I. W. Hamley, A. J. Ryan, W. Bras, K. Almdal, and K. Mortensen, Polyisoprene-polystyrene diblock copolymer phase diagram near the order-disorder transition, *Macromolecules* **28**(26), 8796–8806 (1995).

[14]K. I. Winey, D. A. Gobran, Z. Xu, L. J. Fetters, and E. L. Thomas, Compositional dependence of the order-disorder transition in diblock copolymers, *Macromolecules* **27**(9), 2392–2397 (1994).

[15]H. Hasegawa, H. Tanaka, K. Yamasaki, and T. Hashimoto, Bicontinuous microdomain morphology of block copolymers. 1. tetrapod-network structure of polystyrene- polyisoprene diblock polymers, *Macromolecules* **20**(7), 1651–1662 (1987).

[16]J. N. Owens, I. S. Gancarz, J. T. Koberstein, and T. P. Russell, Investigation of the microphase separation transition in low-molecular-weight diblock copolymers, *Macromolecules* **22**(8), 3380–3387 (1989).

[17]D. A. Hajduk, P. E. Harper, S. M. Gruner, C. C. Honeker, G. Kim, E. L. Thomas, and L. J. Fetters, The gyroid: a new equilibrium morphology in weakly segregated diblock copolymers, *Macromolecules* **27**(15), 4063–4075 (1994).

[18]R. J. Spontak, S. D. Smith, and A. Ashraf, Dependence of the obdd morphology on diblock copolymer molecular weight in copolymer/homopolymer blends, *Macromolecules* **26**(5), 956–962 (1993).

[19]D. A. Hajduk, P. E. Harper, S. M. Gruner, C. C. Honeker, E. L. Thomas, and L. J. Fetters, A reevaluation of bicontinuous cubic phases in starblock copolymers, *Macromolecules* **28**(7), 2570–2573 (1995).

[20]M. W. Matsen and M. Schick, Stable and unstable phases of a diblock copolymer melt, *Physical Review Letters* **72**(16), 2660 (1994).

[21]M. W. Matsen and M. Schick, Self-assembly of block copolymers, *Current Opinion in Colloid & Interface Science* **1**(3), 329–336 (1996).

[22]F. S. Bates and G. H. Fredrickson, Block copolymers—designer soft materials, *Physics today* **52**(2), 32–38 (1999).

[23]J. Vavasour and M. Whitmore, Self-consistent field theory of block copolymers with conformational asymmetry, *Macromolecules* **26**(25), 7070–7075 (1993).

[24]F. S. Bates, M. F. Schulz, A. K. Khandpur, S. Förster, J. H. Rosedale, K. Almdal, and K. Mortensen, Fluctuations, conformational asymmetry and block copolymer phase behaviour, *Faraday Discussions* **98**, 7–18 (1994).

[25]D. A. Hajduk, H. Takenouchi, M. A. Hillmyer, F. S. Bates, M. E. Vigild, and K. Almdal, Stability of the perforated layer (pl) phase in diblock copolymer melts, *Macromolecules* **30**(13), 3788–3795 (1997).

[26]S. Qi and Z.-G. Wang, On the nature of the perforated layer phase in undiluted diblock copolymers, *Macromolecules* **30**(15), 4491–4497 (1997).

[27]M. W. Matsen, T. M. Beardsley, and J. D. Willis, Fluctuation-corrected phase diagrams for diblock copolymer melts, *Physical Review Letters* **130**(24), 248101 (2023).

[28]J.-F. Sadoc and R. Mosseri, Quasiperiodic frank-kasper phases derived from the square-triangle dodecagonal tiling, *Structural Chemistry* **28** (2017).

[29]Https://www.chemie-biologie.uni-siegen.de/ac/hjd/lehre/ss08/vortraege /mehboob_tetrahedrally_close_packing_corr_.pdf,

[30]V. F. Degtyareva and N. S. Afonikova, Structurally complex frank–kasper phases and quasicrystal approximants: electronic origin of stability, *Crystals* **7**(12), 359 (2017).

[31]K. D. Dorfman, Frank–kasper phases in block polymers, *Macromolecules* **54**(22), 10251–10270 (2021).

[32]G. M. Grason, B. DiDonna, and R. D. Kamien, Geometric theory of diblock copolymer phases, *Physical Review Letters* **91**(5), 058304 (2003).

[33]S. Lee, M. J. Bluemle, and F. S. Bates, Discovery of a frank-kasper σ phase in sphere-forming block copolymer melts, *Science* **330**(6002), 349–353 (2010).

[34]K. Momma and F. Izumi, Vesta 3 for three-dimensional visualization of crystal, volumetric and morphology data, *Journal of Applied Crystallography* **44**(6), 1272–1276 (2011).

[35]C. A. Tyler, J. Qin, F. S. Bates, and D. C. Morse, Scft study of nonfrustrated abc triblock copolymer melts, *Macromolecules* **40**(13), 4654–4668 (2007).

[36]A. B. Chang and F. S. Bates, *The abcs of block polymers*, 2020.

[37]M. Liu, W. Li, F. Qiu, and A.-C. Shi, Theoretical study of phase behavior of frustrated abc linear triblock copolymers, *Macromolecules* **45**(23), 9522–9530 (2012).

[38]T. S. Bailey, C. M. Hardy, T. H. Epps, and F. S. Bates, A noncubic triply periodic network morphology in poly (isoprene-b-styrene-b-ethylene oxide) triblock copolymers, *Macromolecules* **35**(18), 7007–7017 (2002).

[39]M. I. Kim, T. Wakada, S. Akasaka, S. Nishitsuji, K. Saijo, H. Hasegawa, K. Ito, and M. Takenaka, Stability of the fddd phase in diblock copolymer melts, *Macromolecules* **41**(20), 7667–7670 (2008).

[40]M. Takenaka, T. Wakada, S. Akasaka, S. Nishitsuji, K. Saijo, H. Shimizu, and H. Hasegawa, Orthorhombic fddd network in diblock copolymer melts,

[41]T. H. Epps, E. W. Cochran, C. M. Hardy, T. S. Bailey, R. S. Waletzko, and F. S. Bates, Network phases in abc triblock copolymers, *Macromolecules* **37**(19), 7085–7088 (2004).

[42]T. H. Epps, E. W. Cochran, T. S. Bailey, R. S. Waletzko, C. M. Hardy, and F. S. Bates, Ordered network phases in linear poly (isoprene-b-styrene-b-ethylene oxide) triblock copolymers, *Macromolecules* **37**(22), 8325–8341 (2004).

[43]C. A. Tyler and D. C. Morse, Orthorhombic f d d d network in triblock and diblock copolymer melts, *Physical Review letters* **94**(20), 208302 (2005).

[44]J. Qin, F. S. Bates, and D. C. Morse, Phase behavior of nonfrustrated abc triblock copolymers: weak and intermediate segregation, *Macromolecules* **43**(11), 5128–5136 (2010).

[45]W. Li, F. Qiu, and A.-C. Shi, Emergence and stability of helical superstructures in abc triblock copolymers, *Macromolecules* **45**(1), 503–509 (2012).

[46]T. P. Lodge, Block copolymers: past successes and future challenges, *Macromolecular Chemistry and Physics* **204**(2), 265–273 (2003).

[47]F. Ganji and M. Abdekhodaie, Synthesis and characterization of a new thermosensitive chitosan–peg diblock copolymer, *Carbohydrate Polymers* **74**(3), 435–441 (2008).

[48]C.-F. Huang, S.-W. Kuo, H.-F. Lee, and F.-C. Chang, A new strategy for the one-step synthesis of block copolymers through simultaneous free radical and ring opening polymerizations using a dual-functional initiator, *Polymer* **46**(5), 1561–1565 (2005).

[49]Y. Lv, Z. Liu, A. Zhu, and Z. An, Glucose oxidase deoxygenation- redox initiation for raft polymerization in air, *Journal of Polymer Science Part A: Polymer Chemistry* **55**(1), 164–174 (2017).

[50]M. Szwarc, M. Levy, and R. Milkovich, Polymerization initiated by electron transfer to monomer. a new method of formation of block polymers1, *Journal of the American Chemical Society* **78**(11), 2656–2657 (1956).

[51]S. Schlick and M. Levy, Block-polymers of styrene and isoprene with variable distribution of monomers along the polymeric chain. synthesis and properties1, *The Journal of Physical Chemistry* **64**(7), 883–886 (1960).

[52]H. Iatrou and N. Hadjichristidis, Synthesis of a model 3-miktoarm star terpolymer, *Macromolecules* **25**(18), 4649–4651 (1992).

[53]L. L. Zhou and J. Roovers, Synthesis of novel carbosilane dendritic macromolecules, *Macromolecules* **26**(5), 963–968 (1993).

[54]N. Hadjichristidis and L. Fetters, Star-branched polymers. 4. synthesis of 18-arm polyisoprenes, *Macromolecules* **13**(1), 191–193 (1980).

[55]R. P. Quirk and F. Ignatz-Hoover, Living coupling agents. rational synthesis of heteroarm star-branched polymers, in Recent advances in anionic polymerization: proceedings of the international symposium on recent advances in anionic polymerization, held april 13–18, 1986 at the american chemical society meeting in new york, new york, usa (Springer, 1987), 393–401.

[56]P. Lutz and P. Rempp, New developments in star polymer synthesis. star-shaped polystyrenes and star-block copolymers, *Die Makromolekulare Chemie: Macromolecular Chemistry and Physics* **189**(5), 1051–1060 (1988).

[57]M. R. Leduc, C. J. Hawker, J. Dao, and J. M. Fréchet, Dendritic initiators for "living" radical polymerizations: a versatile approach to the synthesis of dendritic-linear block copolymers, *Journal of the American Chemical Society* **118**(45), 11111–11118 (1996).

[58]M. W. Matsen and F. S. Bates, Conformationally asymmetric block copolymers, *Journal of Polymer Science Part B: Polymer Physics* **35**(6), 945–952 (1997).

[59]N. Xie, W. Li, F. Qiu, and A.-C. Shi, σ Phase formed in conformationally asymmetric ab-type block copolymers, *Acs Macro Letters* **3**(9), 906–910 (2014).

[60]J. M. White, A. A. Crabtree, F. S. Bates, and M. A. Calabrese, Effect of chain architecture on the structure, dynamics, and rheology of thermoresponsive poloxamer hydrogels and associated blends, *Macromolecules* (2023).

[61]T. P. Lodge, E. Wang, J. Zhu, and F. S. Bates, Solution and bulk structures of asymmetric pep-ps-pep triblock copolymers, *Macromolecules* (2023).

[62]B. Zhang, C. Zheng, F. S. Bates, and T. P. Lodge, Self-assembly of charged diblock copolymers with reduced backbone polarity, *ACS Applied Polymer Materials* **5**(3), 2223–2229 (2023).

[63]J. Xie, C. T. Lai, and A.-C. Shi, Regulating the self-assembly of ab/cd diblock copolymer blends via secondary interactions, *Journal of Polymer Science* (2023).

[64]Y.-T. Juan, Y.-F. Lai, X. Li, T.-C. Tai, C.-H. Lin, C.-F. Huang, B. Li, A.-C. Shi, and H.-Y. Hsueh, Self-assembly of gyroid-forming diblock copolymers under spherical confinement, *Macromolecules* **56**(2), 457–469 (2023).

[65]J. Xie, Y. Li, and A.-C. Shi, Binary blends of diblock copolymers: an efficient route to complex spherical packing phases, *Macromolecular Theory and Simulations* **30**(6), 2100053 (2021).

[66]K. Chen, C.-Y. Chen, H.-L. Chen, R. Komaki, N. Kawakami, T. Isono, T. Satoh, D.-Y. Hung, and Y.-L. Liu, Self-assembly behavior of sugar-based block copolymers in the complex phase window modulated by molecular architecture and configuration, *Macromolecules* **56**(1), 28–39 (2022).

[67]Y. Luo, D. Montarnal, N. J. Treat, P. D. Hustad, M. D. Christianson, E. J. Kramer, G. H. Fredrickson, and C. J. Hawker, Enhanced block copolymer phase separation using click chemistry and ionic junctions, *Acs Macro Letters* **4**(12), 1332–1336 (2015).

[68]J. Kim, H. Y. Jung, and M. J. Park, End-group chemistry and junction chemistry in polymer science: past, present, and future, *Macromolecules* **53**(3), 746–763 (2020).

[69]K. S. Lee, J. Lee, J. Kwak, H. C. Moon, and J. K. Kim, Reduction of line edge roughness of polystyrene-block-poly (methyl methacrylate) copolymer nanopatterns by introducing hydrogen bonding at the junction point of two block chains, *ACS Applied Materials & Interfaces* **9**(37), 31245–31251 (2017).

[70]W. Li, J.-M. Y. Carrillo, B. G. Sumpter, and R. Kumar, Modulating microphase separation of lamellae-forming diblock copolymers via ionic junctions, *ACS Macro Letters* **9**(11), 1667–1673 (2020).

[71]E. Ji, V. Pellerin, L. Rubatat, E. Grelet, A. Bousquet, and L. Billon, Self-assembly of ionizable "clicked" P3HT-b-PMMA copolymers: ionic bonding group/ counterion effects on morphology, *Macromolecules* **50**(1), 235–243 (2017).

[72]H. Lee, J. Kim, and M. J. Park, Exploration of complex nanostructures in block copolymers, *Physical Review Materials* **8**(2), 020302 (2024).

[73]G. Jo, H. Ahn, and M. J. Park, Simple route for tuning the morphology and conductivity of polymer electrolytes: one end functional group is enough, *ACS Macro Letters* **2**(11), 990–995 (2013).

[74]H. Y. Jung, P. Mandal, G. Jo, O. Kim, M. Kim, K. Kwak, and M. J. Park, Modulating ion transport and self-assembly of polymer electrolytes via end-group chemistry, *Macromolecules* **50**(8), 3224–3233 (2017).

[75]H. Lee, S. Kwon, J. Min, S.-M. Jin, J. H. Hwang, E. Lee, W. B. Lee, and M. J. Park, Thermodynamically stable plumber's nightmare structures in block copolymers, *Science* **383**(6678), 70–76 (2024).

[76]G. Fredrickson, *The equilibrium theory of inhomogeneous polymers*, Oxford University Press, New York, 2006.

[77]A. J. Berlinsky and A. B. Harris, *Statistical Mechanics: An Introductory Graduate Course*, Springer Nature, Cham, 2019.

[78]J. Xie, *Self-consistent field theory notes.*

[79]F. S. Bates and G. H. Fredrickson, Block copolymer thermodynamics: theory and experiment, *Annual review of Physical Chemistry* **41**(1), 525–557 (1990).

[80]A. N. Semenov, *Sov. Phys JETP* **61**, 733 (1985).

[81]L. Leibler, Theory of microphase separation in block copolymers, *Macromolecules* **13**(6), 1602–1617 (1980).

[82]A.-C. Shi and J. Noolandi, Effects of short diblocks at interfaces of strongly segregated long diblocks, *Macromolecules* **27**(11), 2936–2944 (1994).

[83]A. Arora, D. C. Morse, F. S. Bates, and K. D. Dorfman, Accelerating self-consistent field theory of block polymers in a variable unit cell, *The Journal of Chemical Physics* **146**(24) (2017).